Fibronectin Module $FN^{III}9$ Adsorption at Contrasting Solid Surfaces Studied by Atomistic Molecular Dynamics

Karina Kubiak-Ossowska[†‡], *Paul A. Mulheran*[†] *and Wieslaw Nowak*[‡*]

[†]Department of Chemical and Process Engineering, University of Strathclyde, James Weir Building, 75 Montrose Street, Glasgow G1 1XJ, United Kingdom

[‡]Institute of Physics, Faculty of Physics, Astronomy and Informatics, Nicolaus Copernicus University, ul. Grudziadzka 5/7, 87-100 Torun, Poland

Corresponding Author: Paul A. Mulheran, paul.mulheran@strath.ac.uk

KEYWORDS: protein adsorption, adsorption mechanism, fibronectin, FN, mica, Au{111}, silica surface, surface diffusion, molecular dynamics simulations, MD.

ABSTRACT:

The mechanism of $FN^{III}9$ fibronectin domain adsorption at pH7 onto various and contrasting surface models has been studied using atomistic molecular dynamics (MD) simulations. We use an ionic model to mimic mica surface charge density, but without a long-range electric field above the surface; a silica model with a long-range electric field similar to that found experimentally; and an Au {111} model with no partial charges or electric field. A detailed description of the adsorption processes and the contrasts between the various model surfaces is provided. In the case of our silica surface with a long-range electrostatic field, the adsorption is rapid and primarily driven by electrostatics. Since it is negatively charged (-1e), $FN^{III}9$ readily adsorbs to a positively charged surface. However, due to its partial charge distribution, $FN^{III}9$ can also adsorb to the negatively charged mica model because of the absence of a long-range repulsive electric field. The protein dipole moment dictates its contrasting orientation at these surfaces, and the anchoring residues have opposite charges to the surface. Adsorption on the model Au {111} surface is possible, but less specific, and various protein regions might be involved in the interactions with the surface. Despite strongly influencing the protein mobility, adsorption at these surfaces does not require wholesale $FN^{III}9$ conformational changes, which suggests that the biological activity of the adsorbed protein might be preserved.

INTRODUCTION

Control of protein adsorption, which will follow detailed understanding of its mechanism, is crucial in modern biology, medicine, and technology.[1] Protein adsorption on the solid artificial surfaces of body implants determines the biological response of a living organism to the implant. Human fibronectin (FN) is a large multi-domain glycoprotein found in insoluble form in the extracellular matrix (ECM) and in soluble form in blood serum.[2,3] While the biological role of ECM FN is to promote cell adhesion and thereby influence cell proliferation, migration, differentiation and growth,[2,3] the soluble form (plasma FN) plays vital roles in blood clotting, wound healing and inflammation response.[3] The molecular shape and conformation depends on its form as well as the environmental conditions. FN's role in cancer progression through interactions with integrin[4] attracts additional interest to this multifunctional protein.[2,3,5] ECM fibronectin is comprised of two, mostly identical, ~250 kDa polypeptide chains connected by two disulphide bridges at the C-termini (C-ter).[6] Each monomer consist of 30 – 32 small, □ – sandwich domains arranged like beads on a string: the smallest FN^{I} (type I; 13 repeats) located at the N- and C-ter; sparse FN^{II} (type II; 2 repeats only) located at the N-ter and surrounded by FN^{I}; and the most numerous FN^{III} (type III; 15-17 repeats) located in the center of the chain and containing a central cell binding domain (CBD) with the amino acid sequence Arg-Gly-Asp (RGD) in repeat 10 (the $FN^{III}10$ domain) and the Pro58-His59-Ser60-Arg61-Asn62 (PHSRN) adhesion synergy region (known as integrin binding region) in repeat 9 ($FN^{III}9$).[2,7,8] Cells are bound through FN interactions with members of the integrin receptors, which are cell-surface receptors that link the ECM with the intracellular cytoskeleton.[2] As well as binding to cells, FN binds to a number of biologically important molecules such as heparin, collagen and fibrin,[2] and also to bacterial proteins. [3]

Due to the size of the protein, FN's detailed three-dimensional structure is not known. Nevertheless, the X-ray structure of the $FN^{III}7B89$ fragment of human FN isoform 1 (domains $FN^{III}7$, $FN^{III}B$, $FN^{III}8$ and $FN^{III}9$; residues 1173 to 1539) has been recently solved,[7] thereby providing new opportunities for molecular dynamics (MD) studies of domain $FN^{III}9$ which is very important in terms of the FN cell adhesion functionality. Furthermore, it is of interest to consider how the FN domains could be used to functionalize material surfaces for biomedical applications. In order to do this, we need to understand how the domains themselves interact with various and contrasting material chemistries, thereby guiding the development of new material systems with potential for new health technologies.

According to the X-ray crystal structure (3T1W.pdb[7]), the $FN^{III}9$ domain shape is ellipsoidal, with a long axis ~40 Å and two short axes each ~30 Å (Fig. 1). Therefore the orientation of the adsorbed protein on the surface might be simplistically described as end-on (with the angle between the protein long axis and the normal to the surface in the range (0^0-30^0), between (31^0-60^0) and side-on (61^0-90^0). Since the N-ter and C-ter are placed on the opposite ends of the ellipsoid, identifying which end is involved in the adsorption is also helpful. In terms of secondary structure, $FN^{III}9$ assumes the classical FN^{III} fold, comprising a sandwich of two antiparallel – sheets with three and four strands,[3,7] (Fig. 1, Tab. S3). In terms of residue type, the protein contains: eight basic (positively charged at pH7) residues - one lysine (Lys85) and seven arginine (Arg33, Arg40, Arg42, Arg51, Arg53, Arg56 and Arg61); and nine acidic (negatively charged) residues - five glutamic acid (Glu46, Glu54, Glu74, Glu86 and Glu87) and four aspartic acid (Asp10, Asp16, Asp19 and Asp55). As a consequence, at pH7 the net protein charge is -1e. We note that there are no cysteine and only one methionine (Met48); these residues can provide sulfur for protein – gold interactions[9].

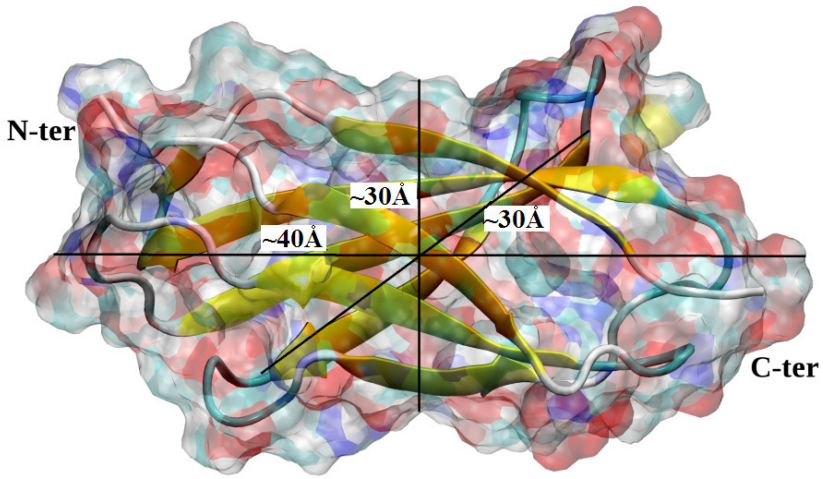

Figure 1. Initial structure of the $FN^{III}9$ domain. The protein surface is indicated as a ghost surface colored by name (C – cyan, H – white, N – blue, O – red, S – yellow), secondary structure is shown as a cartoon colored by a structure type (extended – yellow, turn – cyan, coil – white). The protein ends and dimensions are annotated.

Despite its limitations, namely the simulation time (usually tens to hundreds of nanoseconds are simulated with commonly available computational resources), the system size (the larger molecule, the shorter accessible simulation time) and the forcefield parameterization (the potentials used to describe both bonding and nonbonding interactions of the system), MD simulation has proven its utility to study peptide and protein dynamics in general[10-12] and its adsorption in particular.[13-26] MD can provide a unique insight into the initial adsorption processes. To obtain a more complete picture of the protein activity mechanism and its adsorption, steered MD (SMD) can be used to investigate protein mobility on the surface and its desorption.[27-30] Dissipative particle dynamics,[31] Monte Carlo simulation[32] and coarse grain dynamics[12] provide alternatives, sacrificing atomistic accuracy to access longer time scales. However, to successfully use these techniques one needs to start with accurate adsorption states,

and so fully atomistic MD simulations as presented in this paper are necessary first steps in the investigation of protein surface adsorption.

Early MD studies of the FN^{I} module adsorption on graphite[13] and poly(vinyl alcohol)[14] surfaces were focused on conformational changes upon adsorption and spreading on the surface. More recent MD simulations of FN^{I} module adsorption on polyurethane surfaces,[25] contrary to the aforementioned, indicated formation of β-sheets upon adsorption (the difference might be caused by the explicit water model employed) and pointed out the role of the polymer surface roughness and hydrophilicity. The only adsorption simulations of a FN^{III} module we find in the literature were conducted using a MC method on nanostructured zirconia.[32] There it was found that the initial protein immobilization is a result of the attractive and repulsive electrostatic interactions of basic (Arg/Lys) and acidic (Asp/Glu) residues with the negatively charged sites of the nanostructured surface. Within this model, the binding energy was calculated and the importance of surface roughness was demonstrated. Nevertheless, due to the method used, the detailed adsorption mechanism and the role of non-electrostatic interactions was beyond the reach of the study. MD simulations have been performed on PHSRN peptide (FN's adhesion synergy region) adsorption on hydrophobic and hydrophilic silica, revealing the role of the Arg residue in the adsorption.[24] Earlier SMD studies revealed that the spatial orientation and distance between the adhesion synergy region of $FN^{III}9$ and RDG of $FN^{III}10$ plays a crucial role in their adhesiveness to integrin[27].

Here we present results of systematic, fully atomistic MD simulations of $FN^{III}9$ adsorption on three surface models mimicking those widely used in experimental studies: mica (modeled as a negatively charged ionic surface), silica and gold. We analyze 24 separate adsorption trajectories, each of 100ns duration, in simulation systems carefully designed to probe contrasting behavior at different surface chemistries. The design of the simulation system is

crucial in terms of the electrostatic fields above the surface: employing periodic boundary conditions, we effectively create slit pores with no long range electric field for a model charged ionic surface; by using material models with an intrinsic dipole perpendicular to the surface we create appropriate long-range electric fields above a silica surface; and by using a neutral material model we create an Au{111} surface free from electric fields. Furthermore, the size of the simulation cells and the duration of the trajectories are sufficient to allow the protein to rotate and diffuse to a favorable adsorption orientation, so that the results we present are truly representative of the model systems.

From our trajectories we provide a description of $FN^{III}9$ adsorption, highlighting major differences in the adsorption mechanism on the different types of model surface. The description also focuses on the $FN^{III}9$ module conformational changes, its mobility on the surface, and the $FN^{III}9$ residues exposed to the solvent which may be important for other protein binding. The models we investigate are designed to contrast behavior rather than provide chemical accuracy in the surface interactions. Nevertheless, these insights into the initial adsorption processes will help both the generalization of the protein adsorption mechanism on various surfaces and the design of new materials dedicated to selective protein immobilization and surface functionalization.

MATERIALS AND METHODS

All simulations were performed with the NAMD 2.6[33] package using the Charmm27 force-field, and analyzed using VMD.[34] The initial structure of the $FN^{III}9$ domain of human FN isoform 1 (FN1) was used; the domain was extracted from the $FN^{III}7B89$ fragment structure solved by Schifner *et al*.,[7] PDB code: 3T1W.pdb. The numbering used is "local" e.g. relevant for the $FN^{III}9$ domain only, not for the entire protein.

To obtain the reference trajectory (herein denoted as FNw), the protein was placed in a rectangular box of water molecules (TIP3P model) that extend 29 Å from any protein atom. The net protein charge was -1 e, therefore the system was neutralized by adding NaCl salt with ionic strength of 0.05 M (mol/L); this is suitable ionic strength for experimental work to create functionalized surfaces. The adsorption trajectories were prepared in a similar way, with the surface added in 6 different initial orientations: the surface in the (*x,y*) plane (trajectories denoted as V1 and V2); the (*y,z*) plane (V3 and V4); or the (*x,z*) plane (V5 and V6). In each case, both protein sides initially faced the surface (see Fig. S1 in the Supplementary Materials). The initial protein – surface distance varied between 22.5 Å and 35 Å (the most frequent value was 22.5 Å). We use Periodic Boundary Conditions (PBC), and the initial distance to the image surface varied between 23 – 30 Å, depending on the protein – surface orientation and the surface type used (see below). The number of atoms in each system studied was approximately the same. The systems were subject to 1000 steps of water minimization only followed by 100ps water equilibration at the target temperature 310K. Then the systems (water and protein) were minimized for 10,000 steps, heated for 300 ps to the required temperature and equilibrated at constant temperature for 300 ps. The production MD simulations were pursued for 100 ns at the given temperature in the NVT ensemble. The integration step was 1 fs, the SHAKE algorithm and PBC were used. The cut-off distance for van der Waals interactions was 12 Å, and the smooth particle mesh Ewald (SPME) summation[35,36] was used for the Coulomb interactions. For ionizable residues, the most probable charge states at pH 7 were chosen. No additional restrictions on momentum in the simulations were used.

Surface models

For the mica surface model a single layer of static oxygen and silicon atoms organized into a square array, with charges yielding the density -.027 e/A^2 found experimentally. The surface dimensions were 86.4 Å x 92.8 Å. This model mica surface has been used to reveal key processes in the adsorption of lysozyme,[15-18,21,28] and further details of the model can be found in these papers. The surface was initially placed in the six relative orientations shown in Fig. S1, so we have obtained six 100 ns trajectories denoted FNmV1, … , FNmV6. Due to the PBC and the use of the Ewald summation in this work (in contrast to our previous studies with this model), we note that this surface model produces no long-range electric field and so provides a way to assess adsorption to an ionic surface with local field only.

For the SiO_2 surface model, similarly to our recent work[26] a $\{10\bar{1}\}$ slab of α-cristobalite with dimensions 86 Å x 89 Å x 13 Å was used following Patwardhan *et al.*[23] Two variants of the surface were created: SiO_2 surface with siloxide ($\equiv SiO^-$) groups only on the top and under-coordinated Si species at the bottom and $pSiO_2$ with siloxide groups on the bottom and under-coordinated Si species on the top. The SiO_2 slab model is neutral and stoichiometric, but it has an intrinsic dipole moment across it since we model the material as ions fixed in space. The 3D periodicity of the simulation cell thus creates an electric field across the water/protein space, mimicking the electric field above a single negatively charged silica surface comprising siloxide species[26] (Fig. 2a); the electric field is measured to be 0.2V/A, corresponding to 0.16 charged silanol groups nm^{-2}, comparable to estimates for large silica nanparticles[23]. Details of the force-field parameters for this model can be found in the Supplementary Materials. In the case of $pSiO_2$ shown in Fig. 2b, the silica slabs are inverted so that these simulations can be considered as alternative trajectories for SiO_2 adsorption. Note that in experiments at pH7, the siloxide

groups of the SiO_2 surface are exposed to the solvent, so that our SiO_2 surface, rather than the $pSiO_2$, is actually observed.

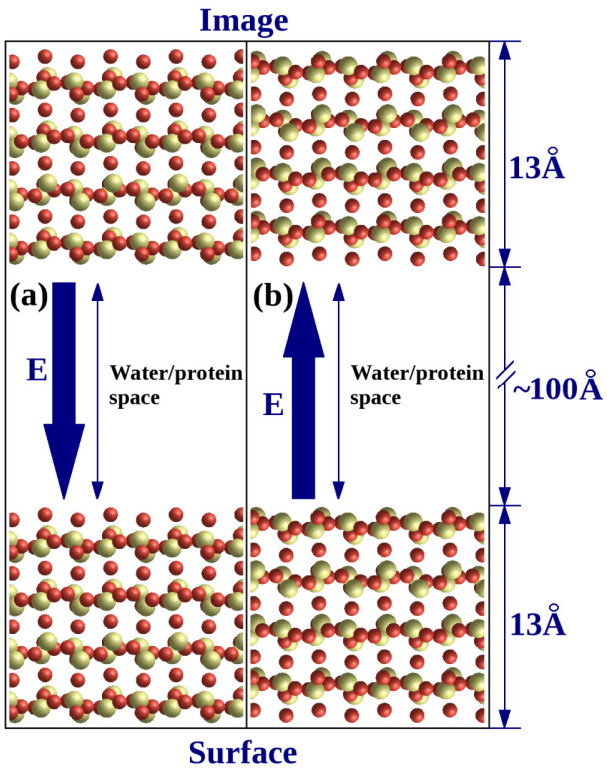

Figure 2. Illustration of the simulation cells and crystal structures used in this study for the SiO_2 and $pSiO_2$ surfaces; silicon is yellow and oxygen is red. (a) The SiO_2 surface: the alpha-cristobalite $\{10\bar{1}\}$ surface is cut so that the upper surface is terminated with under-coordinated oxygen, inducing an electric field E across the water/peptide space due to the dipole moment of the crystal slab. (b) The $pSiO_2$ surface: the slab is flipped vertically.

The close-packed Au {111} surface was constructed by creating a slab of suitably-oriented face-centred cubic crystal (fcc) with lattice parameter 4.078 Å. The slab dimension is 86 Å x 82 Å x 15 Å, containing 5040 atoms, oriented so that the {111} surface is perpendicular to

the z-axis in the simulation cell. The Charmm27 force-field parameters for gold atoms were used accordingly to Heinz *et al.,*[37-39] yielding a hydrophilic gold {111} surface. This can be considered as a model van der Waals surface, with strong surface-protein interactions that can induce a soft epitaxy effect. [C1] The gold atoms were kept immobile during the simulation. The Au {111} surface was initially placed in six various positions with respect to the protein, therefore we have obtained six 100 ns trajectories denoted as FNAuV1, …, FNAuV6.

Summarizing, we have obtained and analyzed 24 adsorption trajectories on three various surfaces (100 ns long each) and compared the protein behavior with a 100 ns reference trajectory with protein in water only.

RESULTS AND DISCUSSION

Adsorption Simulations at the Mica Surface Model

In the case of the $FN^{III}9$ adsorption simulations at the mica surface model (a charged ionic surface with no long-range electric field across the simulation cell due to the use of PBC and the SPME), we have obtained and analyzed six 100 ns trajectories denoted as FNmV1, …, FNmV6. The general protein dynamics, and the adsorption mechanism in particular, were common for all trajectories; the exemplar FNmV3 trajectory (FNmV3.avi) together with the initial orientation of the protein and the close view of the adsorbed state are available in the Supplementary Materials (Fig. S2), while the final orientation of the adsorbed protein is shown in Fig. 3. The initial distance to the protein-surface separation was 22.5 Å, while its final value is 2.2 Å.

In general, in the initial stages of the simulation the protein rotates to orient its dipole moment perpendicular to the surface, so that the angle between the surface normal and the dipole moment is ~180^0. This results in the N-ter region of the FN being exposed to the surface. The protein is then attracted to the surface, with the (N-ter) Lys85 side chain oriented towards the

surface. The protein adsorbs using Lys85 between 4.8 ns and 26.0 ns depending on trajectory; however in this initial adsorption stage, the protein is still mobile on the surface. The attraction to the surface results in the adsorption of other residues, namely the N-ter arginine and serine. In addition to Lys85, which is crucial for the adsorption at the charged surface model, the most important anchors in order of importance are: Arg56, Ser84, Arg51, Arg61 (see Tab. S2 in the Supplementary Materials). The protein is immobilized once it is anchored to the surface by two or three residues, which is observed between 31.2 ns and 98.0 ns depending on trajectory. A particular residue is considered to be adsorbed and anchoring the protein if its separation from the surface becomes consistently smaller than 6 Å.

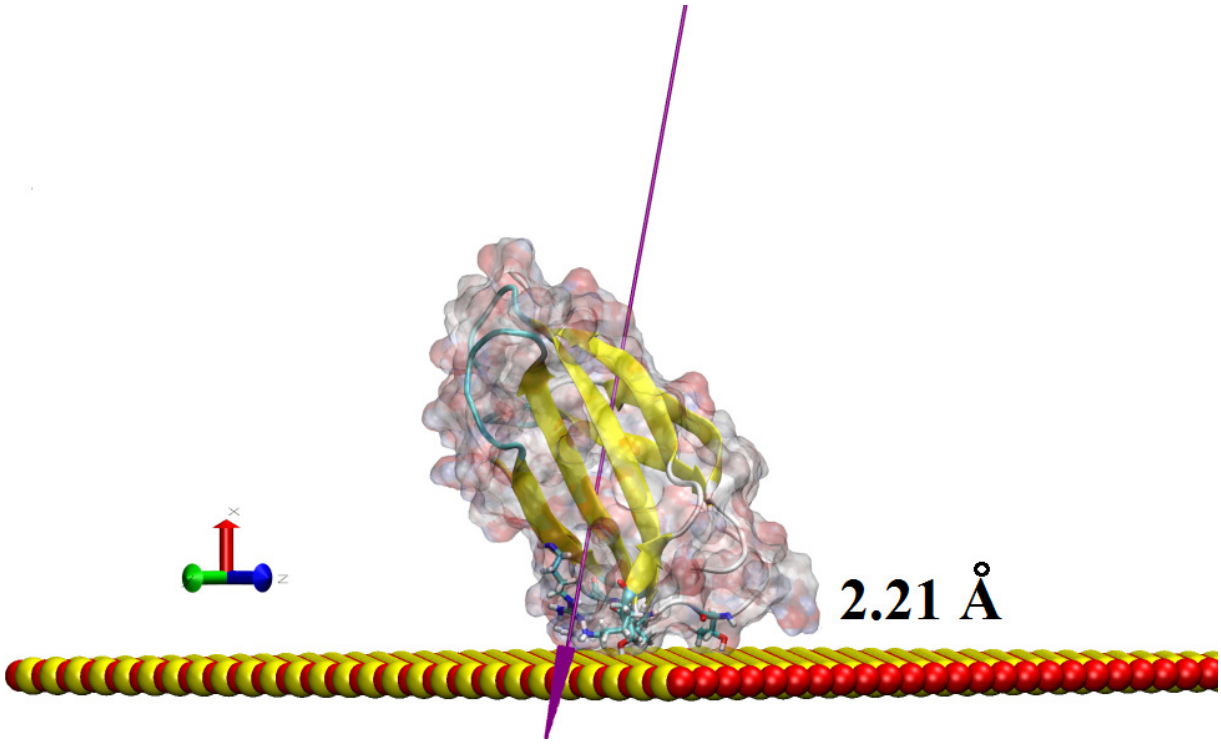

Figure 3. Final adsorption state for the representative trajectory FNmV3 after 100 ns. The FN surface is indicated as a ghost surface colored by charge (blue – positive charges, red – negative, white – neutral), secondary structure is shown as a cartoon colored by structure type (yellow – extended structures, cyan – turns, white – coils), the anchoring residues are shown by licorice

colored by name (C – cyan, H – white, N – blue, O – red). The surface atoms are shown by VdW spheres or CPK colored by type (O red, Si – yellow). The magenta needle indicates the protein dipole moment, and key anchoring residues and their distance from the surface are annotated. Water molecules are not shown for clarity in the pictures.

To quantify the protein orientation on the surface, the angle between its long axis and the surface normal is used. Since the initially adsorbed $FN^{III}9$ can translate on the charged surface model and also rock and swing whilst attached to the surface, all possible orientations (side-on, between and end-on) are observed in the final, strongly adsorbed stages of various trajectories. The minimum protein-surface distance at this stage is ~2.2 Å, while the distance between the protein center of mass (COM) and the surface is ~22 Å regardless of the protein orientation on the surface. The factors influencing the COM distance to the surface include the extent of local conformational protein changes upon adsorption. Consequently, it can be difficult to determine the orientation based on this distance alone.

The overall protein conformation does not significantly change upon adsorption, as suggested both by visual analysis and the RMSD and RMSF plots (for details see the Supplementary Materials); changes are restricted to local structural adjustments in the protein regions closest to the surface, rather than global conformational changes (see also Tab. S3). It is worth noting that almost all the important anchor residues are located in flexible turn (T) or coil (C) regions, and only Arg56 is part of an extended β-structure (B). Examination of the Ramachandran map (data not shown) indicates that all anchor residues are in the allowed regions (i.e. the backbone angles of anchor residues are within the range of the typical values), so that adsorption does not lead to untypical residue conformation. Therefore only local structural

changes are induced by the adsorption, which agrees well with previous MD adsorption studies.[15-18,21,22,26]

Of the anchoring residues, lysine and arginine are positively charged, and serine is polar. Alongside the dipole moment reorientation, this suggests that in the case of adsorption at the model mica surface the driving force is electrostatic and other forces are negligible. This observation agrees well with our previous adsorption simulations for lysozyme on mica.[15-18,21]

We have also analyzed the $FN^{III}9$ region exposed to the solvent in the adsorbed protein state, since it may affect the binding affinity of other proteins to the immobilized FN. The details are listed in the Supplementary Materials Table S4; in general, the $FN^{III}9$ regions exposed to the solvent are the N&C-ter and β-sheets B1 and B7. The region is acidic and neutral in terms of hydrophobicity.

Adsorption Simulations at the SiO_2 Surface

In the case of the $FN^{III}9$ adsorption simulations at the SiO_2 surface, we have obtained and analyzed twelve 100 ns trajectories denoted as $FNSiO_2V1$, …, $FNSiO_2V6$ and $FNpSiO_2V1$, … , $FNpSiO_2V6$. Note that the SiO_2 and $pSiO_2$ systems are alternatives for each other. Since the general protein dynamics and the adsorption mechanism in particular were common for all trajectories, trajectory $FNSiO_2V5$ is used as a representative example. The movie for this trajectory ($FNSiO_2V5$.avi) together with the initial orientation of the protein and the close view of the adsorbed state are available in the Supplementary Materials (Fig. S3), while the final orientation of the adsorbed protein is shown in Fig. 4. The initial distance to the surface was 22.4 Å while the final was 4.36 Å (because of the surface architecture it is not possible for the protein to approach closer than this).

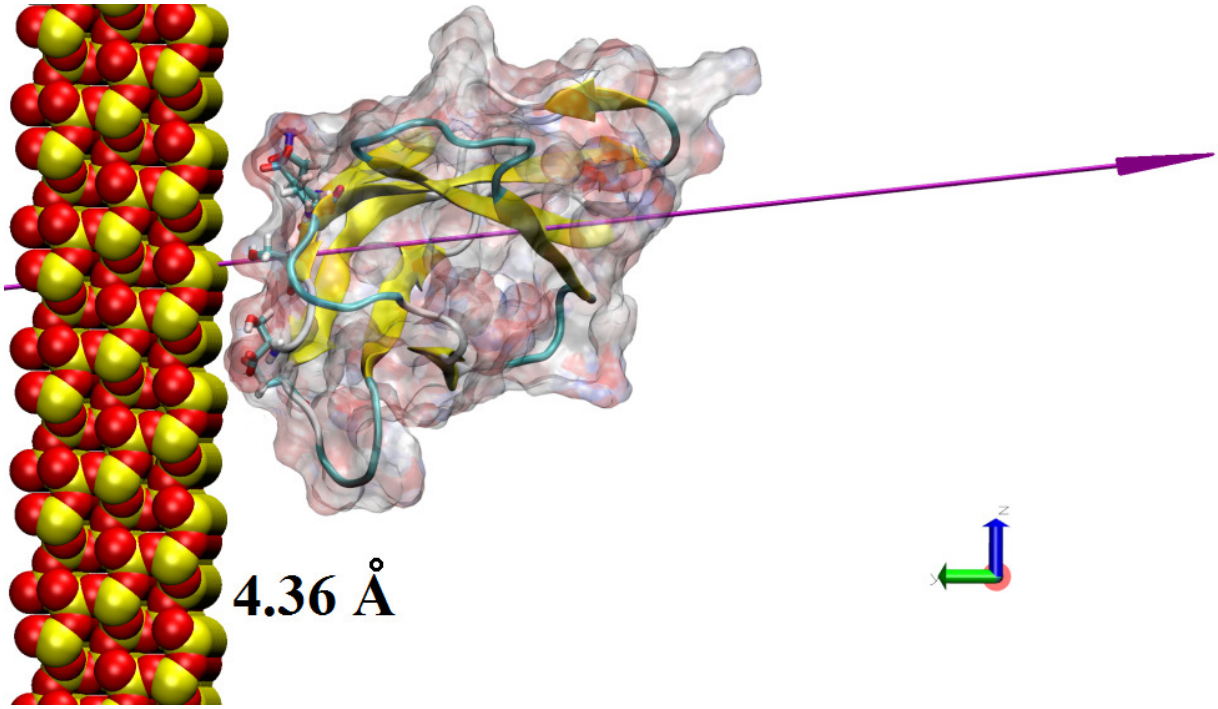

Figure 4. Final adsorption state for the representative trajectory FNSiO$_2$V5. The coloring scheme is the same as in Figure 3.

Among all 12 of these SiO_2 trajectories, the FN^{III}9 has never adsorbed to the siloxide-rich surface, which is the one exposed to solution in experiments. Instead, in all our trajectories, the FN^{III}9 has adsorbed to the surface containing under-coordinated Si species, which is to be expected given the FN^{III}9 net negative charge (-1e). Therefore, we might speculate that FN^{III}9 does not easily adsorb to unmodified SiO_2 surfaces in experiments, nor indeed to mica, which are negatively rather than positively charged at pH7. Rather, our adsorption simulations indicate the behavior expected at model positively charged ionic surfaces, in contrast to the absorption on model negatively charged surfaces described above. We also note that details of the counter-ion adsorption to these surfaces is worthy of further study to see how they might affect these conclusions;[23] this will be done in future work.

In all trajectories the protein rotates to orient its dipole moment perpendicularly to, and away from, the surface containing the under-coordinated Si species, so that the angle between protein dipole moment and surface normal ~0^0 . After this the $FN^{III}9$ is attracted to the surface, with a major role in the attraction played by the C-terminus (Ser99) and in particular it's COO^- group. The Ser99 adsorbs between 4.8 ns and 14.8 ns depending on trajectory, nevertheless in this initial adsorption stage the $FN^{III}9$ is still mobile on the surface. Further attraction to the surface results in other residues adsorbing, mainly aspartic and glutamic acid. Apart from Ser99, which is the crucial for adsorption at the under-coordinated SiO_2 surface model, the most important anchors are Asp19, Asp16, Ser96, and Glu74 (see Table S2). Therefore, the acidic groups are the most important for adsorption on the under-coordinated SiO_2 surface; the partial charges on this surface are positive, and so the adsorption seems to be driven mainly by electrostatic interactions between $FN^{III}9$ and the surface. This is in line with previous MC simulations which highlighted the crucial role of electrostatic complementarity between $FN^{III}9$ and a zirconia surface, and in particular the role of charged residues.[32] We find that Ser96 interacts with the surface by its side chain oxygen, not its hydrogen, so that polarisation might also be important in this case. The protein becomes immobilized when at least three strong contacts with the surface are established; this immobilization is observed between 12 ns and 62 ns depending on trajectory.

To adsorb at the under-coordinated SiO_2 surface, the $FN^{III}9$ always uses its C-ter face and the most typical final orientation at the surface might be described as between, with angle ~45^0 between the protein long axis and the surface normal. Both the side-on and the end-on orientation appeared once in different trajectories, reflecting internal protein flexibility rather than other effects. As seen in Fig. 4, the minimal protein – surface distance in the adsorbed stage of the $FNSiO_2V5$ trajectory was 4.36 Å, while the COM distance to the surface was ~18 Å. Similar

values were obtained for the other trajectories. Again we note that the COM distance to the surface can be affected by local conformational changes upon adsorption. If $FN^{III}9$ could be considered as a hard protein, the COM distance to the surface in end-on orientation would be ~22 Å (half the $FN^{III}9$ length) plus ~5 Å (shortest residue distance to the surface) giving ~27 Å. In the case of side-on orientation the COM distance would be ~15 Å + 5Å =~20Å, while for between orientation the distance should be ~23 Å. Such distances were not observed (for more details see the section below on Protein Mobility on the Surface) because $FN^{III}9$, as with other FN modules, can be classified as a soft protein,[3] and additional conformational changes are expected in the protein part facing the surface. Therefore, the angle between long protein axis and the surface normal seems to be the better indicator of respective orientation on the surface.

Apart from Ser99, which is part of the last coil (C9), the crucial residues are part of extended β-structures (Tab. S3), therefore $FN^{III}9$ structural adjustments close to the surface influence only the local protein structure. Nevertheless, these changes are not very significant, and cannot be considered as unfolding or denaturation. Similar to the mica model surface adsorption described above, all the anchor residues were in allowed regions of the Ramachandran map.

In the final, adsorbed state the region exposed to the solvent comprises N-ter, β-strands B4 and B5, and parts of B3 and B6. The region is basic and hydrophilic (Tab. S4).

Adsorption Simulations at the Au {111} Surface

We have obtained and analyzed six 100 ns trajectories denoted as FNAuV1, …, FNAuV6. Since the protein adsorption at the gold surface is not very specific, two example trajectories (FNAuV1.avi and FNAuV5.avi) together with the initial orientation of the protein and close views of the adsorbed states are available in the Supplementary Materials (Fig. S4), while the

final orientations of the adsorbed protein are shown in Fig. 5. In contrast to the mica and SiO_2 model surfaces, the Au{111} surface slab does not possess a dipole moment and the gold atoms are not partially charged, therefore electrostatic forces are not expected to play a crucial role in the protein adsorption.

Despite the low specificity of the adsorption at the Au{111} surface, we are still able to identify some general features during the $FN^{III}9$ adsorption at this surface. Because of the lack of strong electrostatic forces driving the protein onto the surface, the diffusion stage prior to adsorption is longer than in the previous systems. The first adsorption event is usually observed much later than in the case of adsorption at the model mica or SiO_2 surfaces, but it can also happen after only 4.8 ns (Tab. S2). The same applies to the immobilization on the surface. Moreover, in one trajectory (FNAuV4) adsorption is not observed at all, the protein is only close to the surface after 100 ns dynamics. During its long, free diffusion in the solute, the protein occasionally comes closer to the surface, and if its distance from the surface falls below 12 Å the $FN^{III}9$ starts to feel the Lenard-Jones surface potential. At this stage, the protein can be slowly attracted to the surface, in the orientation which occurred by chance in its earlier diffusion. For this reason, $FN^{III}9$ adsorbs at the Au{111} surface by its N-ter or C-ter if the final orientation on the surface is end-on, and by using both termini if the final orientation is side-on (Tab. S2). The distance between the protein COM and the surface varies between 15 Å and 30 Å, depending on the trajectory, while the smallest protein – gold distance is ~ 2.3 Å (Fig. 5). Because of the low adsorption specificity, a common trend is not observed in terms of the residues exposed to the solvent (see Tab. S4).

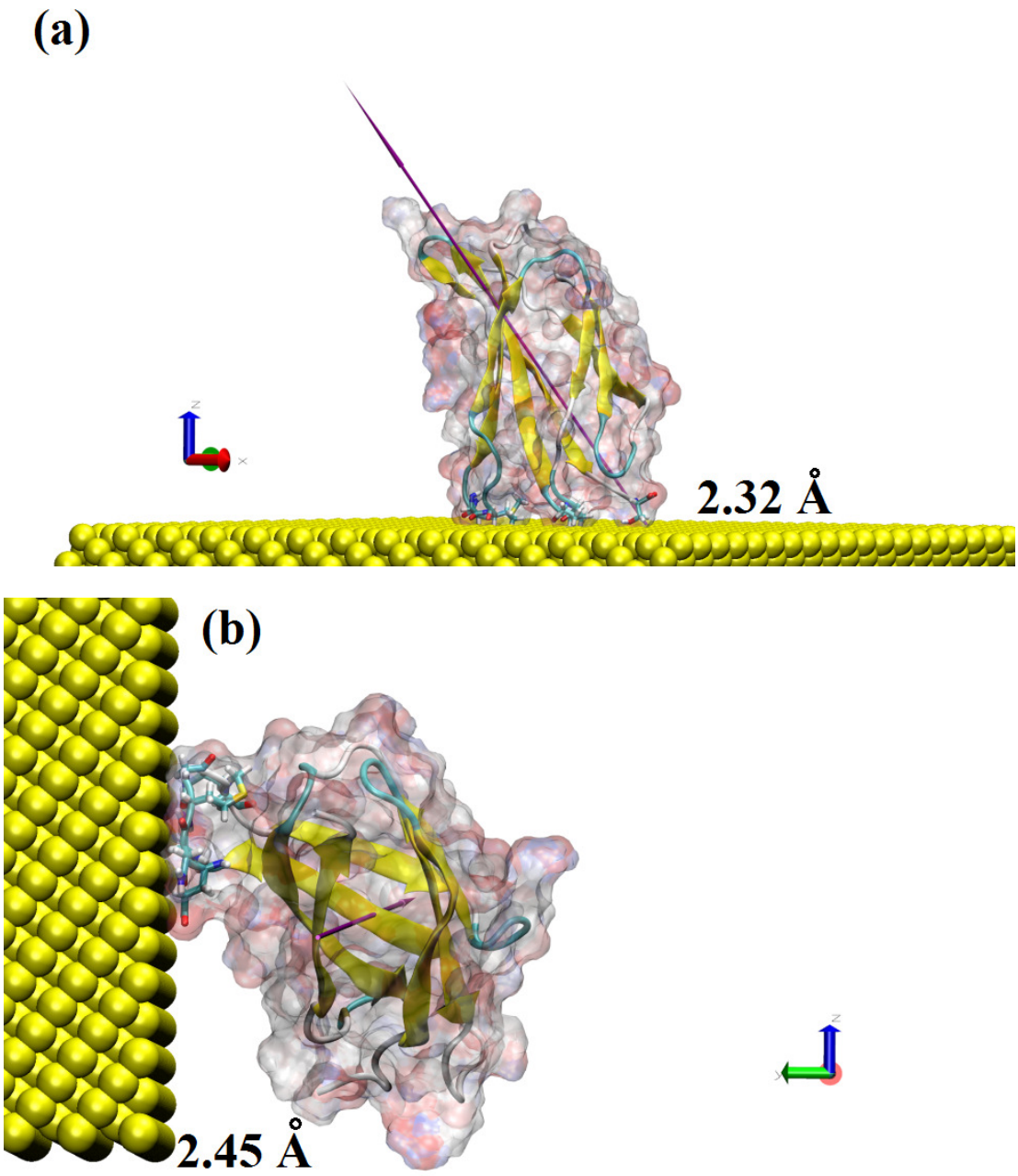

Figure 5. Final adsorption states for the representative trajectories FNAuV1 and FNAuV5. The coloring scheme is the same as on Figure 3, gold is shown in yellow.

The list of crucial residues for $FN^{III}9$ adsorption at the model Au{111} surface comprises [a]Asn23 (T), [a]Asn47 (T), [a]Met48 (T), [a]Arg51 (T/C), [b]Lys85 (T), [b]Glu86 (B/T), and [b]Glu87 (B).

The residues [c]Ala8 (N-ter, C), [c]Ser99 (C-ter, C), [c]Thr21 (T), [c]Thr35 (C), [a]Arg40 (B), [a]Arg42 (B), [b]His44 (B), [b]Glu46 (T), [b]Glu54 (B), [a]Arg56 (B), [a]Asn68 (C/T), [c]Gly72 (T/C) and [a]Asn83 (B/T/C) also seem to be important. In letters in brackets indicate the secondary structure from which the residue comes: B is an extended structure, C is a coil, and T is a turn. The notation B/T/C indicates that the secondary structure of the particular residue varies between trajectories, for more details see Supplementary Table S3. The superscript denotes residues with the highest (a), intermediate (b) and the lowest (c) affinity to Au{111} surface accordingly to Feng *et al.*[38] The Ramachandran map indicates that all anchor residues in the adsorbed state are in allowed regions. Apart from Met48, all the anchor residues are hydrophilic or neutral; electrostatic forces are ruled out as a driving force for adsorption on this model gold surface, whilst surface complementarity effects are apparent in line with the parameters used. [37,38]

The presence of Met48 in the list of important residues in the interactions with the gold surface is worthy of more consideration. The role of another sulfur-containing residue, cysteine, for gold nanoparticle creation on the protein matrix has been discussed.[9] It is possible that metionine's sulphur, despite its lower accessibility, can play a similar role. We note that in sulphur – gold interactions, electronic effects are crucial and our classical MD simulations cannot access this information in detail. Nevertheless, from the MD results presented here, it might be worthwhile investigating the interactions of methionine with gold on an electronic structure level. A poly-$FN^{III}9$ construct, investigated with AFM techniques, may also be useful here.

The residues involved in the protein – Au{111} surface interactions come from coils, turns as well as structures, therefore it might be expected that local structural adjustments and conformational changes would impact on the global protein structure. Nevertheless, as discussed in detail in the next section, the Au{111} surface-induced conformational changes are comparable with the intrinsic protein flexibility.

Structural Changes Upon Adsorption

$FN^{III}9$ is a mostly structure protein[7] which contains 8 extended structures (7 -sheets and one short structure, for details see Tab.S3) connected by coils and turns which are responsible for the relatively significant intrinsic flexibility. Details of structural changes upon adsorption at all of the studied model surfaces, provided in the Supplementary Materials, confirm that $FN^{III}9$ is a flexible module. This intrinsic flexibility is one of the factors which allows effective adsorption, so that unfolding is not required. Similar behavior has been observed for hen egg white adsorption on the model mica surface.[15-18,21] Moreover, the results presented here agree well with previous MD simulations of FN^{I} adsorption on a polyurethane surface[25] where even some folding events on the surface were detected. However these contradict MD simulations results of FN^{I} adsorption on poly(vinyl alcohol) and graphite[13,14] surfaces, where total protein unfolding and spreading was observed. The inconsistency between these computational studies is probably due to the use of implicit water models in the early MD studies, whereas we explicitly include water molecules in our work. Numerous experimental studies reported reversible, full length FN unfolding upon adsorption.[41-45] This reversibility suggests changes in module location with respect to one another, rather than unfolding of the FN modules themselves; in other words, changes in the tertiary and quaternary structures of the full FN protein rather than in the separate modules' secondary structure.

Protein Mobility on the Surface

Another issue of wide interest is the protein mobility on the surface. The reduction of the protein mobility by the surface can be visualized in the COM traces shown in Figure 6. The protein mobility is strongly reduced by the adsorption, even in its initial stage (when protein is “trapped”

by the surface and interacts by one to three residues acting as anchors), and the immobilized adsorption stage substantially reduces the COM mobility on the surface. During the initial stage protein is relatively mobile on the surface, the position and orientation of each anchor can change spontaneously, desorbing and re-adsorbing independently from one another. This process is mainly facilitated by side chain flexibility, and it usually affects neither the backbone structure of the protein nor the part of the protein facing the surface. It is worth noting that the simultaneous desorption of all anchors has not been observed in any of our simulations, so that even in the very initial adsorption state, $FN^{III}9$ was not able to desorb. During the initial adsorption period, the main structural adjustments of the protein region facing the surface are also observed; they start even whilst the first anchor is being attracted to the surface. Once three or more residues establish a strong interaction with the surface, so they no longer desorb individually, the $FN^{III}9$ adsorption state can be considered as immobilized. In this stage translations and rotations are noticeably reduced, nevertheless small local changes at the protein region facing the surface are still observed.

For comparison, Figure 6e shows the COM trace calculated for the trajectory within which adsorption has not been observed (FNAuV4). In this case the protein came closer to the image of the Au{111} surface (due to the gold slab construction this is chemically equivalent to the gold surface itself), establishing some interaction, but the separation from the surface remains too large to be categorized as adsorption.

In all the adsorbed protein cases, the amplitude of the immobilized protein movement is usually not smaller than 6 Å and can reach 14 Å (~half of protein size) within 30 ns of reaching the immobilized state, which suggests that the adsorbed protein is flexing on the surface. The apparently higher mobility for the protein adsorbed on SiO2 (Fig. 6b) is just an artifact caused by this flexing.

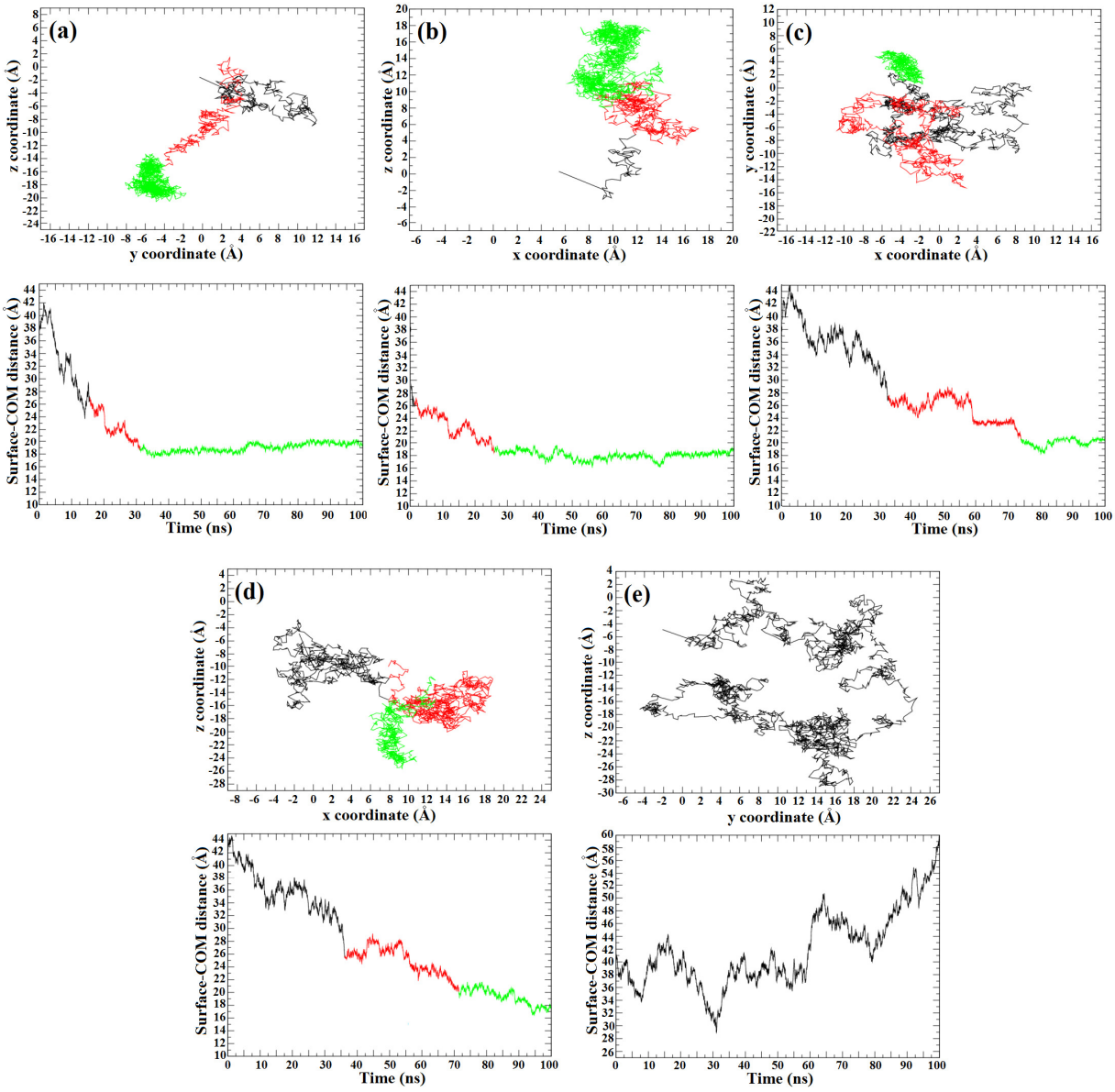

Figure 6. $FN^{III}9$ center of mass (COM) diffusion: (a) FNmV3, (b) $FNSiO_2V5$, (c) FNAuV1, (d) FNAuV5, (e) FNAuV4. The top plots show plan views of the diffusion across the plane of the surface. The black part of the plot indicates the diffusion before adsorption, the red part indicates the diffusion on the surface during the initial stage of adsorption, and the green part indicates the diffusion of $FN^{III}9$ immobilized on the surface. The bottom plots show changes in time of the COM distance perpendicular to the surface, the same coloring scheme is used.

CONCLUSIONS

In this work we have presented a series of fully atomistic MD simulations of $FN^{III}9$ fibronectin module adsorption at various model surfaces. We employed simulation cells designed for a model ionic mica surface, a siloxane-rich SiO_2 surface with an electric field across the water/protein space, and an Au{111} surface without an electric field, allowing us to compare the strength and impact of various forces on $FN^{III}9$ adsorption.

We have found that adsorption driven by electrostatic forces is more direct and specific then adsorption driven by alternative interactions (such as surface complementarity on the gold surface model). In the former case, the 100 ns time scale is long enough to observe all crucial events during the early stages of protein adsorption, while in the latter case such a time scale is not always adequate, although the adsorption events we see are sufficient to characterize the process.

The adsorption mechanism at the electrically charged surfaces is relatively fast due to strong electric forces and requires initial redirection of protein dipole moment (through protein rotations), followed by small conformational adjustments on the protein region facing the surface. At the first stage of the adsorption, when only one residue interacts with the surface, the protein is mobile on the surface, and this mobility is noticeably reduced once more than two or three residues start to act as anchors. Since $FN^{III}9$ adsorbs to under-coordinated Si species, instead of siloxide ($\equiv SiO^-$) groups exposed to the solute, we can conclude that $FN^{III}9$ adsorption at SiO_2 surface under experimental conditions is not very probable. The same will therefore be true for real mica, which also is negatively charged with an associated long-range electric field at physiological conditions. The usual protein orientation at the surface is called as between, e. g. the angle between protein long axis and surface normal is ~45^0.

In the absence of a strong electric field, as in the case of the gold surface, the adsorption is observed to be less specific. The weakness of the forces results in the fact that in one of our 6 trajectories the $FN^{III}9$ has not adsorbed, and in two of our trajectories it has not been immobilized on the surface. Among residues interacting with the Au{111} surface, those with positive and negative charges are found, as are hydrophobic, hydrophilic and neutral residues. The low adsorption specificity on gold has been also found by other authors and can potentially lead to difficulties with parameterization of the protein-gold interactions.[37-40,46,47] Since hydrophobic Met48 is incorporated in protein – gold interactions, we hypothesize that this might indicate an important role for sulfur-gold interactions.

The adhesion synergy region, important for R5ß1integrin-mediated adhesion, is not involved in the surface interaction, therefore the biological activity of $FN^{III}9$ is likely to be retained upon adsorption. Conformational changes of the $FN^{III}9$ module observed upon adsorption are related to local structural adjustments and intrinsic module flexibility than protein unfolding. A summary of the residues easily accessed by solvent is provided in the Supplementary Materials.

It should be emphasized that with the classical MD approach we have only accessed the early adsorption states and in principle, as we have recently shown, the stable adsorption state can slightly differ[28] from this early picture. Nevertheless, by focusing on model systems designed to draw out the contrasting behavior at differing surface chemistries, our simulations elucidate numerous issues and indicate further directions of research, such as the role of sulfur in gold surface interactions and adsorption at more realistic positively charged oxide surfaces.

ACKNOWLEDGMENT

This work was supported by NCN grant no. N202 262038 (WN). Results were obtained using the EPSRC funded ARCHIE-WeSt High Performance Computer (www.archie-west.ac.uk); EPSRC grant no. EP/K000586/1. Authors would like to thank Karolina Mikulska – Ruminska for help in choosing the initial simulation structure of FN.

Supporting Information Available

Movies showing $FN^{III}9$ adsorption on all surface models in illustrative orientations, details of the SiO_2 surface model parameters together with protein – surface relative orientation at the initial trajectory stages, summary of the adsorption trajectories (including the list of major anchor residues and the adsorption time), comparison of the adsorption mechanism at various surfaces together with the figures showing the initial orientation and the close view of the final (adsorbed) structures, table listing protein secondary structure, analysis regarding residues accessibility to the solvent and details regarding $FN^{III}9$ structural changes upon adsorption. This material is available free of charge via the Internet at http://pubs.acs.org.

REFERENCES

1. Huebsch, N.; Mooney, D. J. Inspiration and Application in the Evolution of Biomaterials. *Nature* **2009**, 462, 426-432.

2. Pankov, R.; Yamada, K. M. Fibronectin at Galance, *J. Cell. Sci.* **2002**, 115, 3861-3863.

3. Henderson, B.; Nair, S.; Pallas, J.; Williams, M. A. Fibronectin: a Multidomain Host Adhesin Targeted by Bacterial Fibronectin-Binding Proteins. F*EMS Microbiol. Rev.* **2011**, 35, 147-200.

4. Jia, D.; Entersz, I.; Butler, C; Foty, R. A. Fibronectin Matrix-Mediated Cohesion Suppresses Invasion of Prostate Cancer Cells. *BMC Cancer* **2012**, 12, 94.

5. Mosher, D. F.; Furcht, L. T. Fibronectin: Review of its Structure and Possible Functions. *J. Invest. Dermatology* **1981**, 77, 175-180.

6. Hohenester, E; Engel, J. Domain Structure and Organization in Extracellular Matrix Proteins. *Matrix Biol.* **2002**, 21, 115-128.

7. Schiefner, A.; Gebauer, M.; Skerra, A. Extra-domain B in Oncofetal Fibronectin Structurally Promotes Fibrillar Head-to-tail Dimerization of Extracellular Martix Protein. J. *Biol. Chem.* **2012**, 287, 17578-17588.

8. Redick, S. D; Settles, D. L., Briscoe, G.; Erickson, H. P. Defining Fibronectin's Cell Adhesion Synergy Site by Site-Directed Mutagenesis. *J. Cell Biol.* **2000**, 149, 521-527.

9. Xie, J.; Zheng, Y.; Ying, J. Y. Protein-Directed Synthesis of Hightly Fluorescent Gold Nanoclusters. *J. Am. Chem. Soc.* **2009**, 131, 888-889.

10. Kubiak, K; Nowak, W. Molecular Dynamics Simulations of the Photoactive Protein Nitrile Hydratase. *Biophys. J.* **2008**, 94, 3824-3838.

11. Sanders, J.M.; Wampole, M. E.; Thakur, M. E.; Wickstrom, E. Molecular Determinants of Epidermal Growth Factor Binding: A Molecular Dynamics Study. *PLoS ONE.* **2013**, 8, e54136

12. Yu, H.; Schulten, K. Membrane Sculpting by F-BAR Domains Studied by Molecular Dynamics Simulations. *PLoS Comput. Biol.* **201**3, 9, e1002892.

13. Raffaini, G.; Ganazzoli, F. Molecular Dynamics Simulation of Adsorption of a Fibronectin Module on a Graphite Surface. *Langmuir* **2004**, 20, 3371-3378.

14. Raffaini, G.; Ganazzoli, F. Protein Adsorption on the Hydrophobic Surface of a Glassy Polymer: a Computer Simulation Study. *Phys. Chem. Chem. Phys.* **2006**, 8, 2765-2772.

15. Mulheran, P. A; Kubiak, K. Protein Adsorption Mechanisms on Solid Surfaces: Lysozyme-on-mica. *Mol. Sim.* **2009**, *35*, 561-566.

16. Kubiak, K.; Mulheran, P. A. Molecular Dynamics Simulations of Hen Egg White Lysozyme Adsorption at a Charged Solid Surface. *J. Phys. Chem. B* **2009**, *113*, 12189-12200.

17. Kubiak – Ossowska, K.; Mulheran, P. A. What Governs Protein Adsorption and Immobilization at a Charged solid Surface? *Langmuir* **2010**, *26*, 7690-7694.

18. Kubiak – Ossowska, K.; Mulheran, P. A. Mechanism of Hen Egg White Lysozyme Adsorption on a Charged Solid Surface. *Langmuir* **2010**, *26*, 15954 – 15965.

19. Kang, Y.; Li, X.; Yu, Y.; Wang, Q.; Årgen, H. On the Mechanism of Protein Adsorption onto Hydroxylated and Nonhydroxylated TiO_2 Surfaces, *J. Phys. Chem. C* **2010**, 114, 14496-14502.

20. K□ppen, S.; Langel, W. Simulation of Adhesion Forces and Energies of Peptides on Titanium Dioxide Surfaces. *Langmuir* **2010**, 26, 15248-15256.

21. Kubiak – Ossowska, K.; Mulheran, P. A. Multiprotein Interactions during Surface Adsorption: a Molecular Dynamics Study of Lysozyme Aggregation at a Charged Solid Surface. *J. Phys. Chem. B* **2011**, *115*, 8891-8900.

22. Steudle, A.; Pleiss, J. Modelling of Lysozyme Binding to a Cation Exchange Surface at Atomic Detail: The role of Flexibility. *Biophys. J.* **2011**, 100, 3016-3024.

23. Patwardhan, S. V.; Emami, F. S.; Berry, R. J.; Jones, S. E.; Naik, R. R.; Deschaume, O.; Heinz, H.; Perry, C. C. Chemistry of Aqueous Silica Nanopatricle Surfaces and the Mechanism of Selective Peptide Adsorption. *J. Am. Chem. Soc.* **2012**, 134, 6244-6256.

24. Satriano, C.; Fragala, M. E.; Forte, G.; Santoro, A. M.; La Mendola, D.; Kasemo, B.; Surface Adsorption of Fibronectin-Derived Peptide Fragments: the Influence of Electrostatics and Hydrophobicity for Endothelial Cells Adhesion, *Soft Matter* **2012**, 8, 53-56.

25. Panos, M.; Sen, T. Z.; Ahunbay, M.G. Molecular Simulations of Fibronectin Adsorption onto Polyurethane Surfaces. *Langmuir* **2012**, 28, 12619-12628.

26. Kubiak – Ossowska, K; Burley, G.; Patwardhan, S. V.; Mulheran, P. A. Spontaneous Membrane-Translocating Peptide Adsorption at Silica surfaces: A Molecular Dynamics Study, *J. Phys. Chem. B*, **2013**, *B*, **2013**, 117, 14666-14675.

27. Krammer, A.; Craig, D.; Thomas, W. E.; Schulten, K.; Vogel, V. A Structural Model for Force Regulated Integrin Binding to Fibronectin's RGD-Synergy Site, *Matrix Biol.* **2002**, 21, 139-147.

28. Kubiak – Ossowska, K.; Mulheran, P. A. Protein Diffusion and Long-Term Adsorption States at Chatged Solid Surfaces, *Langmuir* **2012**, 28, 15577-15585.

29. Peplowski, L.; Kubiak, K.; Nowak, W. Mechanical Aspects of Nitrile Hydratase Enzymatic Activity. Steered Molecular Dynamics Simulations of Pseudonocardia Thermophilia JCM3095. *Chem. Phys Lett.* **2008**, 467, 144-149.

30. Colizzi, F.; Perozzo, R.; Scapozza, L.; Recanatini, M.; Cavali, A. Single-Molecule Pulling Simulations Can Discern Active from Inactive Enzyme Inhibitors. J. *Am. Chem. Soc.* **2010**, 132, 7361-7371.

31. Paterson, K.; Lisal, M.; Colina, C. M. Adsorption Behavior of Model Proteins on Surfaces, *Fluid Phase Equilib.* **2011**, 302, 48-54.

32. Sabirianov, R. F.; Rubinstein, A.; Navamar, F. Enhanced Initial Protein Adsorption on Engineered Nanostructured Cubic Zirconia. *Phys. Chem. Chem. Phys.* **2011**, 13, 6597-6609.

33. Phillips, J. C.; Braun, R.; Wang, W.; Gumbart, J.; Tajkhorshid, E.; Villa, E.; Chipot, Ch.; Skeel, R. D.; Kale, L.; Schulten K. Scalable Molecular Dynamics with NAMD. *J. Comput. Chem.* **2005**, 26, 1781-1802.

34. Humphrey, W.; Dalke, A; Schulten, K. Visual Molecular Dynamics. *J. Molec. Graphics* **1996**, 14, 33-38.

35. Essmann, U.; Perera, L.; Berkowitz M. L.; Darden, T.; Lee, H.; Pederson, L. A Smooth Particle Mesh Ewald Method. *J. Chem. Phys.* **1995**, 103, 8577-8593.

36. Kastenholz, M. A.; Hünenberger, P. H. Influience of Artificial Periodicity and Ionic Strenght in Molecular Dynamics Simulations of Charged Biomolecules Employing Lattice-Sum Methods, *J. Phys. Chem. B* **2004**. 108, 774-788.

37. Heinz, H.; Farmer, B. L.; Pandey, R. B.; Slocik, J. M.; Patnaik, S. S.; Pachter, R.; Naik, R. R. Nature of Molecular Interactions of Peptides with Gold, Palladium and Pd-Au Bimetal Surfaces in Aqueous Solution. *J. Am. Chem. Soc.*, **2009**, 131, 9704-9714.

38. Feng, J.; Pandey, R. B.; Berry, R. J.; Farmer, B. L.; Naik, R. R.; Heinz, H. Adsorption Mechanism of Single Amino Acid and Surfactant Molecules to Au {111} surfaces in Aquaeous Solution: Design Rules for Metal-Binding Molecules. *Soft Matter*, **2011**, 7, 2113-2120.39. Heinz, H.; Vaia, R. A.; Farmer, B. L.; Naik, R. R. Accurate Simulation of Surfaces and Interfaces of Face-Centered Cubic Metals Using 12-6 and 9-6 Lennard-Jones Potentials. *J. Phys. Chem. C* **2008**, 112, 17281-17290.

40. Wright, L. B.; Rodger, P. M.; Corni, S.; Walsh, T. R. GolP-CHARMM: First-Principles Based Force fields for the Interaction of Proteins with Au(111) and Au(100). *J. Chem. Theory Comput.* **2013**, 9, 1616-1630.41. Lhoest, J.-B.; Detrait, E.; van den Bosch de Aguilar, P.; Bertrand, P. Fibronectin Adsorption, Conformation, and Orientation on Polystyrene Substrates Studied by Radiolabeling, XPS, and ToF SIMS. *J. Biomed. Mater. Res.* **1998**, 41, 95-103.

42. Yang, Y.; Glover, R.; Ong, J. L. Fibronectin Adsorption on Titanium Surfaces and its Effect on Osteoblast Precursor Cell Attachment. *Coll. Surf. B* **2003**, 30, 291-297.

43. Sousa, S. R.; Moradas-Ferreira, P.; Barbosa, M. A. TiO_2 Type Influences Fibronectin Adsorption. *J. Mat. Sci.* **2005**, 16, 1173-1178.

44. Ribeiro, C.; Panadero, J. A.; Sencadas, V.; Lanceros-Mendez, S.; Tamano, M. N.; Mortal, D.; Salmeron-Sanchez, M.; Gomez Ribelles, J. L. Fibronectin Adsorption and Cell Response on Electroactive poly(vinylidene fluoride) films. *Biomed. Matter.* **2012**, 7, 035004.

45. Grinnell, F.; Feld, M. K. Fibronectin Adsorption on Hydrophilic and Hydrophobic Surfaces Detected by Antibody Binding and Analyzed during Cell Adhesion in Serum-containing Medium. *J. Biol. Chem.* **1982**, 257, 4888-4893.

46. Vila Verde, A.; Acres, J. M.; Maranas, J. K. Investigating the Specificity of Peptide Adsorption on gold Using Molecular Dynamics Simulations, *Biomacromolecules,* **2009**, 10, 2118-2128.

47. Rosa, M.; Corni, S.; Di Felice, R. Enthalpy-Entropy Tuning in the Adsorption of Nucleobases at the Au(111) Surface. *J. Chem. Theory. Comput.* **2014**, 10, 1707-1716.

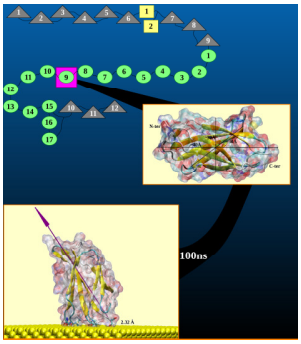

TOC figure. Fibronectin module FN III[9] adsorption at contrasting solid surfaces is studied by atomistic molecular dynamics at 100ns timescale.

Fibronectin Module $FN^{III}9$ Adsorption at Contrasting Solid Surfaces Studied by Atomistic Molecular Dynamics

Karina Kubiak-Ossowska[†‡], *Paul A. Mulheran*[†] *and Wieslaw Nowak*[‡*]

[†]Department of Chemical and Process Engineering, University of Strathclyde, James Weir Building, 75 Montrose Street, Glasgow G1 1XJ, United Kingdom

‡Institute of Physics, Faculty of Physics, Astronomy and Informatics, Nicolaus Copernicus University, ul. Grudziadzka 5/7, 87-100 Torun, Poland

Supplementary Materials

1. Supplementary movies

FNmV3.avi – a movie showing $FN^{III}9$ adsorption on the mica surface model, the most representative trajectory FNmV3 is chosen. The surface atoms are shown by VdW spheres, the protein surface colored by name is shown as a ghost surface, the secondary structure is shown by a cartoon and anchor residues are indicated by licorice. Trajectory length is 100ns, water molecules are not shown. The most important residues, as well as the N- and C-ter, are annotated at the initial and final stages of the trajectory.

$FNSiO_2V5$.avi – a movie showing $FN^{III}9$ adsorption on the SiO_2 surface model, the most representative trajectory $FNSiO_2V5$ is chosen. The surface atoms are shown by VdW spheres, the protein surface colored by name is shown as a ghost surface, the secondary structure is shown by a cartoon and anchor residues are indicated by licorice. Trajectory length is 100ns, water molecules are not shown. The most important residues, as well as the N- and C-ter, are annotated at the initial and final stages of the trajectory.

FNAuV1.avi and FNAuV5.avi – movies showing $FN^{III}9$ adsorption on the Au{111} surface model. Since the adsorption is not as specific as with the other surfaces, two typical trajectories, FNAuV1 and FNAuV5, are chosen. The surface atoms are shown by VdW spheres, the protein surface colored by name is shown as a ghost surface, the secondary structure is shown by a cartoon and anchor residues are indicated by licorice. Trajectory length is 100ns, water molecules are not shown. The most important residues, as well as the N- and C-ter, are annotated at the initial and final stages of the trajectory.

2. Details of the SiO_2 surface model.

In order to simulate the silica surfaces we have parameterized the force-field following the work of Patwardhan *et al.*[1] by adjusting the parameters of the Charmm27 force-field. The parameters we use are summarized in Table S1. The Si-O bonds and Si-O-Si bond angles were not included in the parameterization, since surface silicon and oxygen were fixed in all stages of our MD simulations.

Table S1. Charmm27 force-field parameters used in variants of the α-cristabolite $\{10\bar{1}\}$ slab.

Atom	Charge (e)	ε_0 (kcal/mol)	½ R_0 (Å)
Silicon	+1.10	-0.50	2.00
Oxygen	-0.55	-0.25	1.75

The respective model surface – protein orientations used are shown in Fig. S1.

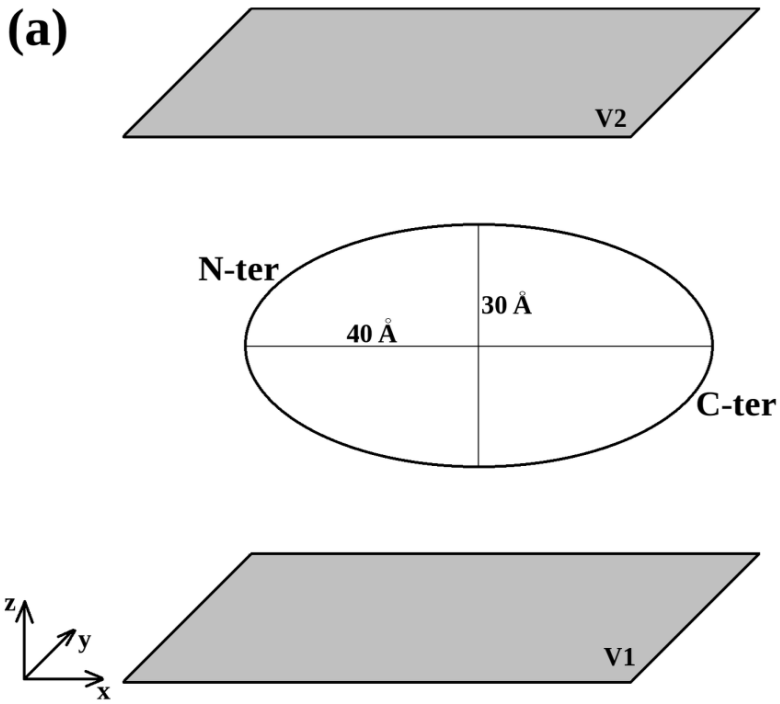

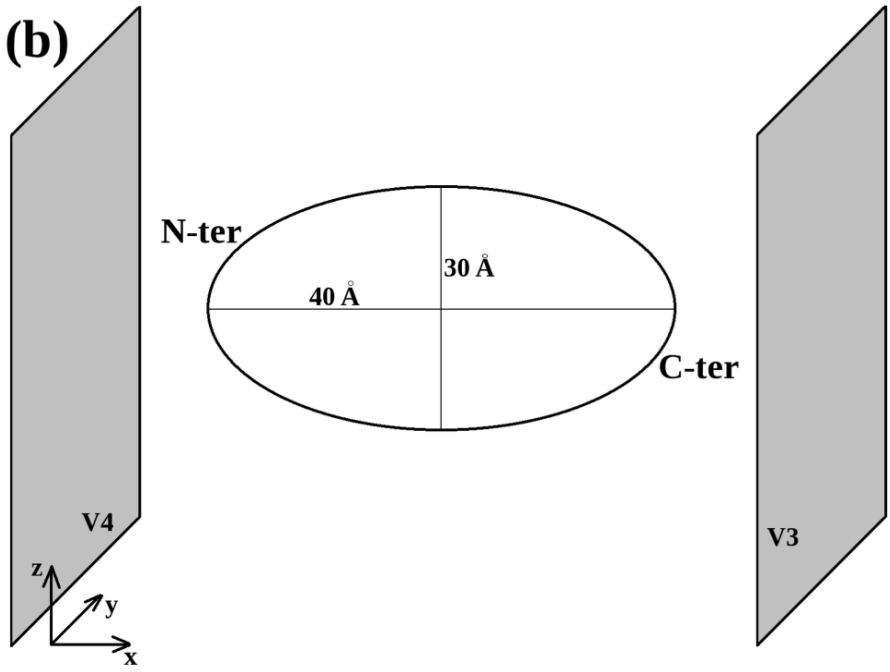

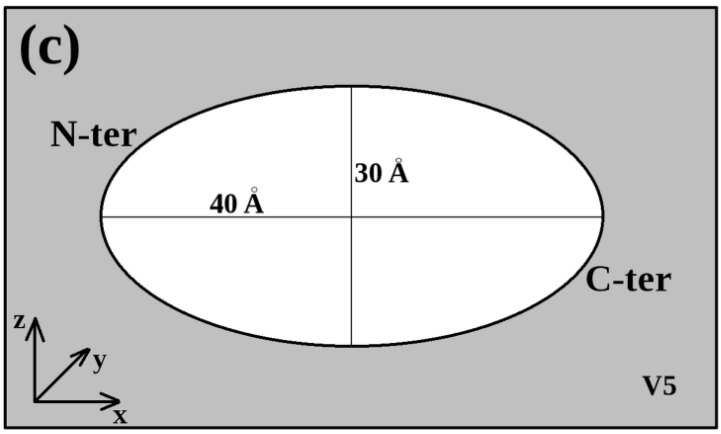

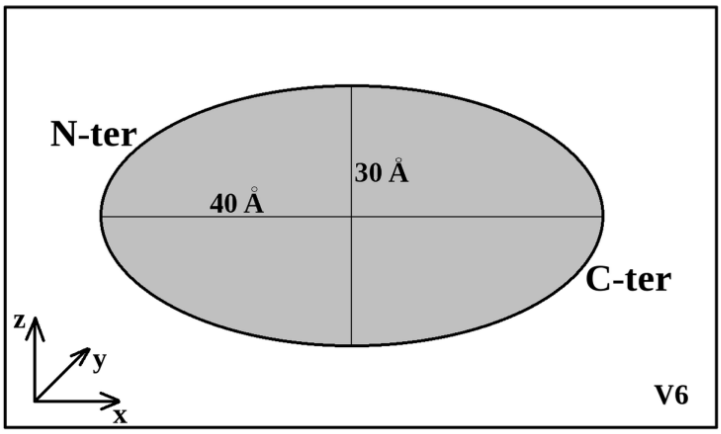

Figure S1. Schematic representation of the initial fibronectin – surface arrangements: (a) Orientation in trajectories denoted as V1 and V2, (b) Orientation in trajectories denoted as V3 and V4, (c) Orientation in trajectories denoted as V5 and V6.

3. Summary of the adsorption trajectories

Table S2. Adsorption trajectories summary. The time (in ns) of the first residue adsorption (A) and protein immobilization (I) is specified together with the list of the most important residues for the protein – surface interaction (main anchors listed in order of importance). In the last column the protein orientation on the surface is specified by providing the angle between the protein long axis and the surface normal together with the protein termini involved in the adsorption. The orientation on the surface is described as end-on if the angle ranges between 0^0 and 30^0, as between if the angle is from 31^0 to 60^0 and as side-on if the angle is from 61^0 to 90^0. Trajectories denoted by * are chosen as representative ones.

Trajectory		Time		Main anchors	Orientation
		A	I		
FNm	V1	26.0	72.0	Lys85, Arg56, Arg51, Arg61	Side-on, 700, by N-ter
	V2	20.0	98.0	Lys85, Arg56, Arg51, Arg61	Between, 450, by N-ter
	V3*	15.6	31.2	Lys85, Ser84, Arg56, Thr37, Arg61, Thr35	End-on, 200, by N-ter
	V4	4.8	74.8	Lys85, Arg51	Side-on, 700, by N-ter
	V5	23.2	54.4	Lys85, Ser84	End-on, 1600, by N-ter
	V6	21.2	66.0	Lys85, Arg51, Arg53, Arg56, Arg40	Side-on, 700, by N-ter
$FNSiO_2$	V1	14.8	40.0	Ser99, Asp19, Ser96, Asp16, Glu74, Asn47, Glu46	Between, 450, by C-ter
	V2	4.4	24.8	Ser99, Asp19, Ser96, Glu74, Glu46, Asn47, Gly72	End-on, 300, by C-ter
	V3	12.4	29.0	Ser99, Asp19, Ser96, Glu74, Asn47, Glu46, Gly72,	Between, 450, by C-ter
	V4	3.6	43.2	Ser99, Asp19, Glu74, Ser96, Asp16, Gly72, Thr97	Between, 450, by C-ter
	V5*	1.2	26.0	Ser99, Asp19, Glu74, Gln94	Between, 450, by C-ter
	V6	13.2	34.0	Ser99, Asp19, Glu74, Ser96, Glu46	Between, 450, by C-ter
$FNpSiO_2$	V1	6.8	36.0	Ser99, Asp19, Glu74, Asp16	Between, 450, by C-ter
	V2	12.0	27.2	Ser99, Asp19, Glu74, Ser96, Gly72, Thr21, Asn23	Between, 450, by C-ter
	V3	6.0	12.0	Ser99, Asp19	End-on, 200, by C-ter
	V4	14.4	28.0	Ser99, Asp19, Ser96, Gln94	Between, 450, by C-ter

	V5	8.4	62.0	Ser99, Asp19, Ser96, Glu74	Side-on, 700, by C-ter
	V6	4.8	31.2	Ser99, Asp19, Ser96, Glu74	Between, 450, by C-ter
FNAu	V1*	32.8	74.0	Ser99, aMet48, aAsn47, cGly72	End-on, 300, by C-ter
	V2	95.2	–	aAsn23	End-on, 300, by C-ter
	V3	64.4	83.6	bLys85, aAsn23, bGlu86. Ala8, cThr35,	End-on, 200, by N-ter
	V4	–	–	Ser99, aAsn68, aAsn23, cThr21	End-on, 300, by C-ter
	V5*	36.1	71.4	Ser99, aMet48, aArg51, cGly49, aAsn47	Side-on, 800 ,N&C-ter
	V6	4.8	28.8	bLys85, aArg51, aArg40, aArg42, bHis44, bGlu46, aAsn47, aMet48, cGly49, cGly50, bGlu54, aArg56, bGlu86, bGlu87	Side-on, 800 , N&C-ter

According to Feng *et al.,*[2] a denotes amino acids with the highest affinity to gold {111} surface (52% of all anchors detected), b denotes amino acids with the intermediate affinity (27%) and c denotes amino acids with the lowest affinity (21%). Note, Ala8 and Ser99 are excluded since they are terminal residues.

4. Comparison of the Adsorption Mechanisms

The general scenario of $FN^{III}9$ adsorption on charged surfaces with long-range electric fields above them might be described as follows: (1) redirection of the protein dipole moment to align in the electric field through protein rotation and slight structural changes; (2) initial adsorption by a charged residue (positive or negative, depending on the surface charge); (3) further slight structural changes (adjustments) at the protein part facing the surface; (4) adsorption of other anchor residues; (5) protein immobilization on the surface. In the case of adsorption at the model mica surface the first anchor involved in step (2) is Lys85, while the residues involved in step (4) are: Arg56, Arg51 and Arg61. In the case of the SiO2 surface, in step (2) C-te Ser99 is involved (possessing negative charge on the backbone), while in step (4) Asp19, Asp16 and Glu74 are involved, although from Tab. S2 the list of residues involved in step (4) can be slightly modified.

The adsorption scenario on the electrically neutral Au{111} surface is as follows: (1) free diffusion; (2) accidental reduction of the protein – surface separation (in our simulation the critical value is 12 Å, but this is artificially imposed by our potential cut-off, so in reality it might be

larger); (3) slow attraction to the surface; (4) slight structural changes of the protein region facing the surface; (5) initial adsorption by Ser99 (C-ter), Asn23/Asn47 (soft epitaxy group a) or Lys85 (group b) (6) further slight structural changes; (7) other anchor adsorption; (8) protein immobilization. The role of Met48, the only sulfur-containing residue of FNIII9, also seems to be important.

The adsorption rate strongly depends on the surface characteristics; in general the larger the surface charge density, the more rapid the adsorption. If the surface has a long-range electric field (as in our SiO2 model), electrostatic forces dominate the adsorption and other interactions do not seem to be important. Similarly, if the surface is ionic but without the long-range electric field (as in our mica model), electrostatics again dominates. Nevertheless, weaker forces can also drive the adsorption in the absence of a strong electrostatic field. In this case the adsorption rate is significantly reduced.

As Table S2 indicates, despite incorporation of Asn, Arg, Ser and His residues, none of the PHSRN located at the protein surface is involved in the interactions with the surfaces we studied. This suggests that biological activity is maintained in surface immobilized FNIII9 modules. Nevertheless, to support this thesis additional simulations are required to confirm the possibility of integrin binding to adsorbed FNIII9. The list of solvent accessible residues is given in Table S4.

5. Initial and Final Adsorption Stage Figures

The initial and final adsorption states obtained for the representative trajectories: FNmV3; $FNSiO_2V5$; FNAuV1 and FNAuV5 are shown in Figures S2, S3 and S4, respectively.

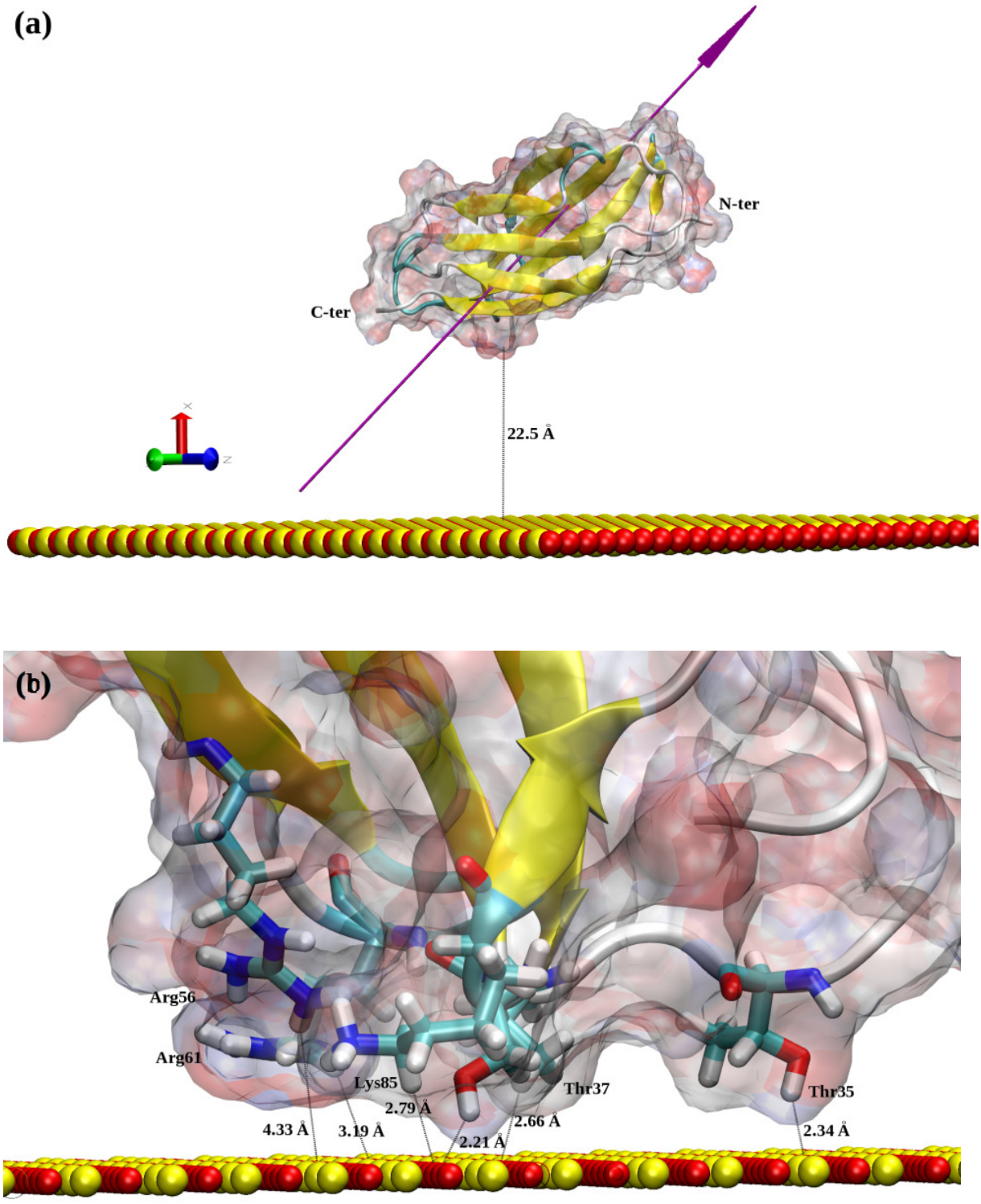

Figure S2. Initial and final adsorption state for the representative trajectory FNmV3. (a) Initial protein – surface oriantetion, (b) close view showing protein – surface interactions after 100 ns of the trajectory. The FN surface is indicated as a ghost surface colored by charge (blue – positive charges, red – negative, white – neutral), secondary structure is shown as a cartoon colored by structure type (yellow – extended β structures, cyan – turns, white – coils), the anchoring residues

are shown by licorice colored by name (C – cyan, H – white, N – blue, O – red). The surface atoms are shown by VdW spheres or CPK colored by type (O red, Si – yellow). Key anchoring residues and their distance from the surface are annotated. Water molecules are not shown for clarity in the pictures.

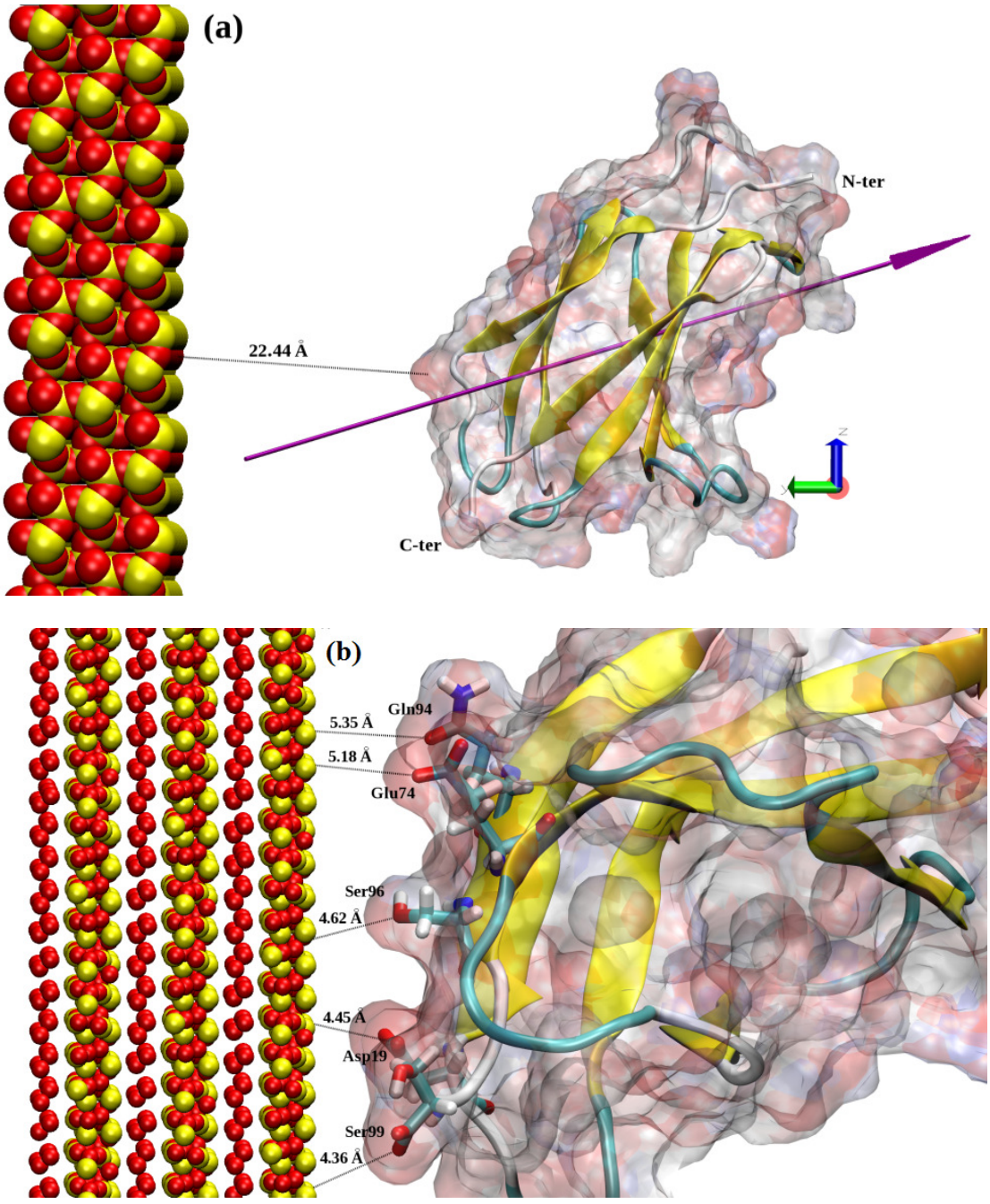

Figure S3. Initial and final adsorption state for the representative trajectory FNSiO$_2$V5. (a) Initial protein – surface oriantetion, (b) close view showing protein – surface interactions after 100 ns of the trajectory. The coloring scheme is the same as in Fig. S2.

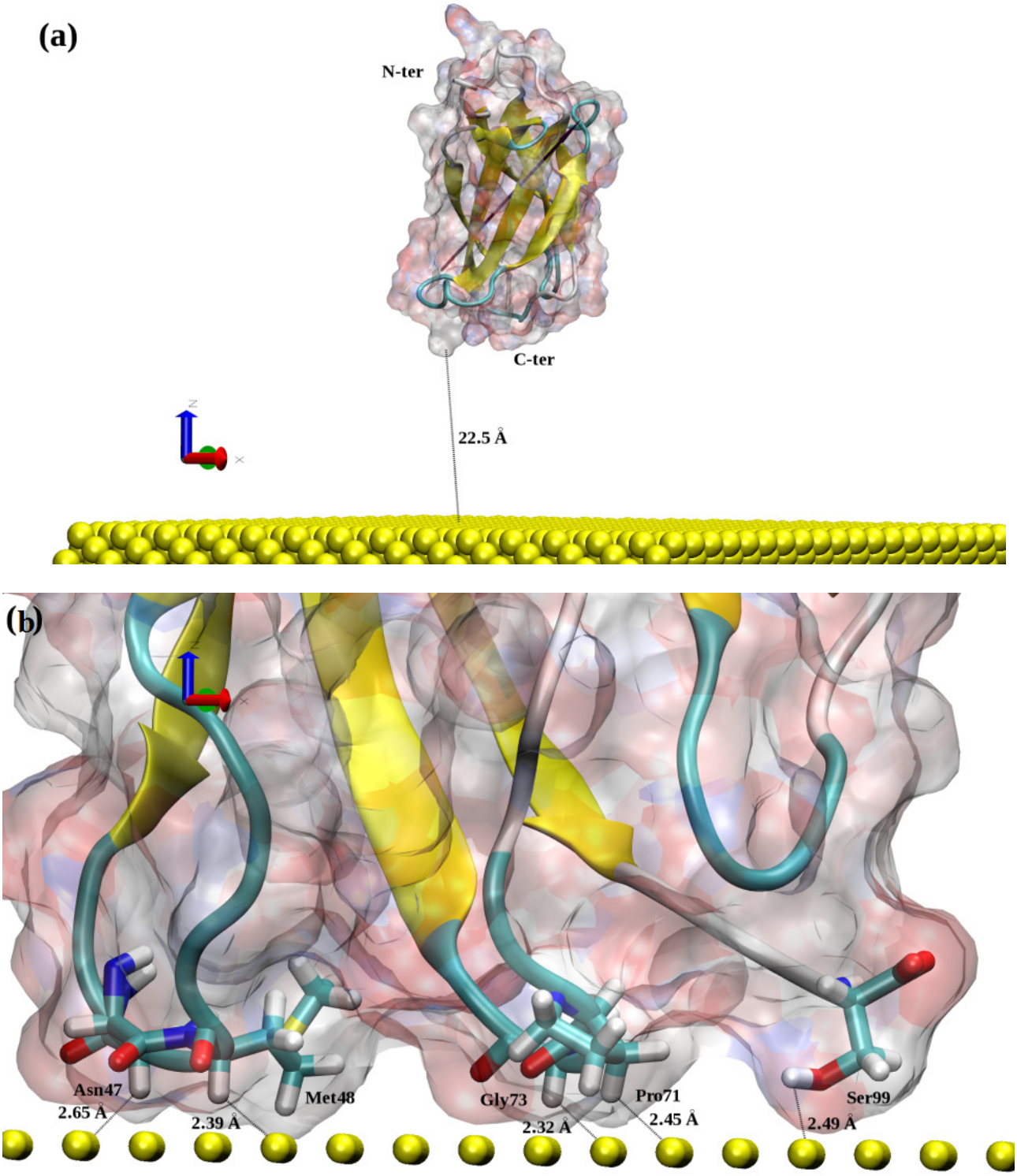
(a)
N-ter
C-ter
22.5 Å
(b)
Asn47
2.65 Å
2.39 Å
Met48
Gly73
2.32 Å
Pro71
2.45 Å
Ser99
2.49 Å

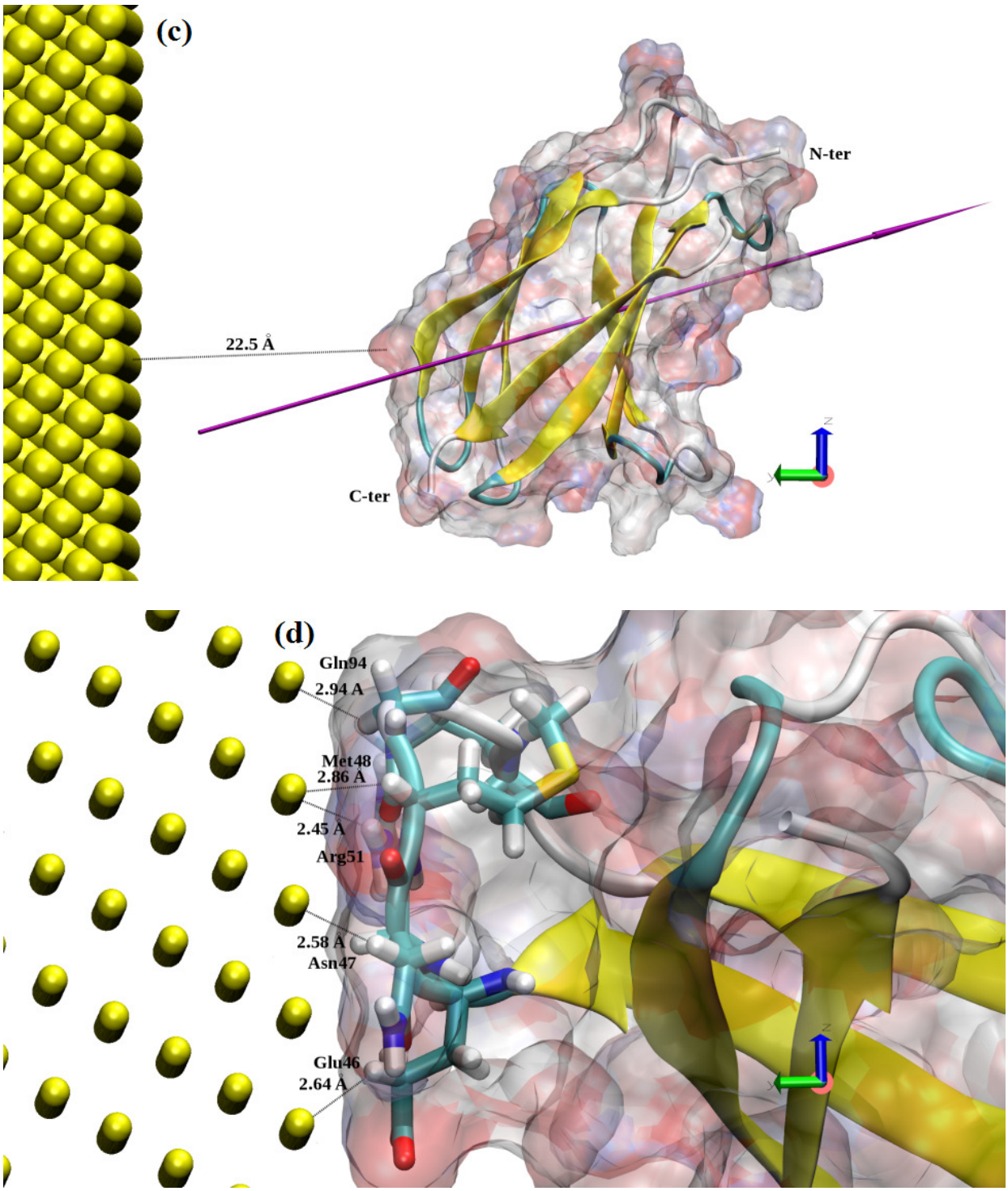

Figure S4. Initial and final adsorption state for the representative trajectories FNAuV1 and FNAuV5. (a) FNAuV1 Initial protein – surface orientation, (b) FNAuV1 close view showing protein – surface interactions after 100 ns of the trajectory, (c) FNAuV5 initial protein – surface orientation and (d) FNAuV5 close view showing protein – surface interactions after 100ns of the trajectory. The coloring scheme is the same as in Fig. S2.

6. Secondary Structure Table

Table S3. Secondary structure of all $FN^{III}9$ residues. Structure elements are coded by symbols and colours: grey – coil (C), blue – turn (T), yellow - extended β-sheet, red (Bb) – β-bridge. The second column lists the secondary structure of the initial protein, and the number of the structure element is given in brackets. The third column summarizes the secondary structure after 100ns in water only (FNw), while the next 24 give the secondary structure in the adsorbed $FN^{III}9$ from the trajectories on mica (FNm), SiO_2 ($FNSiO_2$ and $FNpSiO_2$) and gold (FNAu) surface models. Colour coding is additionally used in the first column to indicate the role of the residues in the adsorption. Residues important for adsorption on mica are highlighted by green (crucial) and olive green (other anchors); those important for adsorption on SiO_2 are highlighted by raspberry pink (crucial) and pink (other anchors). In the case of gold, the adsorption is not specific and all anchor residues seem to be more or less equally important, they are highlighted by light blue.

Residue	Trajectory																									
	Initial	FNw	FNm						$FNSiO_2$						$FNpSiO_2$						FNAu					
			V1	V2	V3	V4	V5	V6	V1	V2	V3	V4	V5	V6	V1	V2	V3	V4	V5	V6	V1	V2	V3	V4	V5	V6
Ala8	C(1)	C	C	C	T	C	C	C	C	C	C	C	C	C	C	C	C	C	C	C	C	C	C	C	C	C
Leu9	C(1)	C	C	C	T	C	C	C	C	C	C	C	C	C	C	C	C	C	C	C	C	C	C	C	C	C
Asp10	C(1)	C	C	C	T	C	C	C	C	C	C	C	C	C	C	C	C	C	C	C	C	C	C	C	C	C
Ser11	C(1)	C	C	C	T	C	C	C	C	C	C	C	C	C	C	C	C	C	C	C	C	C	C	C	C	C
Pro12	C(1)	C	C	C	T	C	C	C	C	C	C	C	C	C	C	C	C	C	C	C	C	C	C	C	C	C
Thr13	B(1)	B	B	B	B	B	B	B	B	B	B	Bb	B	B	B	B	B	Bb	B	B	B	B	B	B	B	B
Gly14	B(1)	B	B	B	B	B	B	B	B	B	B	C	B	B	B	B	B	C	B	B	B	B	B	B	B	B
Ile15	B(1)	B	B	B	B	B	B	B	B	B	B	C	B	B	B	B	B	C	B	B	B	B	B	B	B	B

Asp16	B(1)	B	B	B	B	B	B	B	B	B	B	C	B	B	B	B	B	B	B	B	B	B	B	B	B	B
Phe17	B(1)	B	B	B	B	B	B	B	B	B	B	C	B	B	B	B	B	B	B	B	B	B	B	B	B	B
Ser18	B(1)	B	B	B	B	B	B	B	C	C	T	C	B	C	B	B	C	C	B	C	B	B	B	C	B	C
Asp19	C(2)	Bb	C	C	B	B	B	B	C	C	T	C	B	C	B	B	C	C	B	C	B	B	B	C	B	C
Ile20	C(2)	T	C	C	B	B	B	B	T	T	T	C	B	T	B	T	C	T	B	T	B	B	B	C	B	T
Thr21	T(1)	T	T	T	T	T	T	T	T	T	T	T	T	T	T	T	C	T	T	T	T	T	T	C	T	T
Ala22	T(1)	T	T	T	T	T	T	T	T	T	T	T	T	T	T	T	C	T	T	T	T	T	T	C	T	T
Asn23	T(1)	T	T	T	T	T	T	T	T	T	T	T	T	T	T	T	C	T	T	T	T	T	T	C	T	T
Ser24	T(1)	C	T	T	T	B	T	C	C	C	T	T	C	C	T	C	C	C	T	C	T	T	T	C	T	C
Phe25	B(2)	C	B	B	B	B	B	B	C	C	B	C	B	C	B	B	C	C	B	C	B	B	B	C	B	C
Thr26	B(2)	B	B	B	B	B	B	B	B	B	B	Bb	B	B	B	B	B	B	B	B	B	B	B	C	B	B
Val27	B(2)	B	B	B	B	B	B	B	B	B	B	C	B	B	B	B	B	B	B	B	B	B	B	C	B	B
His28	B(2)	B	B	B	B	B	B	B	B	B	B	C	B	B	B	B	B	B	B	B	B	B	B	C	B	B
Trp29	B(2)	B	B	B	B	B	B	B	B	B	B	C	B	B	B	B	B	B	B	B	B	B	B	C	B	B
Ile30	B(2)	B	B	B	B	B	B	B	B	B	B	Bb	B	B	B	B	B	Bb	B	B	B	B	B	C	B	B
Ala31	C(3)	C	C	C	C	C	C	C	C	C	C	C	C	C	C	C	C	Bb	C	C	C	C	C	C	C	C
Pro32	C(3)	C	C	C	C	C	C	C	C	C	C	C	C	C	C	C	C	C	C	C	C	C	C	C	C	C
Arg33	C(3)	C	C	C	C	C	C	C	C	C	C	C	C	C	C	C	C	C	C	C	C	C	C	C	C	C
Ala34	C(3)	C	C	C	C	C	C	C	C	C	C	C	C	C	C	C	C	C	C	C	C	C	C	C	C	C
Thr35 Thr35	C(3)	C	C	C	C	C	C	C	C	C	C	C	C	C	C	C	C	C	C	C	C	C	C	C	C	C
Ile36	C(3)	C	C	C	C	C	C	C	C	C	C	C	C	C	C	C	C	C	C	C	C	C	C	C	C	C
Thr37	C(3)	C	C	C	C	C	C	C	C	C	C	C	C	C	C	C	C	C	C	C	C	C	C	C	C	C
Gly38	B(3)	B	B	B	B	B	B	B	B	C	B	B	B	B	B	B	B	B	B	B	B	B	B	B	B	B
Tyr39	B(3)	B	B	B	B	B	B	B	B	B	B	B	B	B	B	B	B	B	B	B	B	B	B	B	B	B

Arg40	Arg40	B(3)	B	B	B	B	B	B	B	B	B	B	B	B	B	B	B	B	B	B	B	B	B	B	B	B	B
Ile41		B(3)	B	B	B	B	B	B	B	B	B	B	B	B	B	B	B	B	B	B	B	B	B	B	B	B	B
Arg42		B(3)	B	B	B	B	B	B	B	B	B	B	B	B	B	B	B	B	B	B	B	B	B	B	B	B	B
His43		B(3)	B	B	B	B	B	B	C	B	B	B	B	B	B	B	B	B	B	B	B	B	B	B	B	B	B
His44		B(3)	B	B	B	B	B	B	C	B	B	B	B	B	B	B	B	B	B	B	B	C	B	B	B	B	B
Pro45		B(3)	B	B	B	B	B	B	T	Bb	B	B	T	B	T	B	B	T	B	B	B	T	B	T	T	B	T
Glu46	Glu46	T(2)	T	T	T	T	T	T	T	T	T	T	T	T	T	T	T	T	T	T	T	T	T	T	T	T	T
Asn47	Asn47	T(2)	T	T	T	T	T	T	T	T	T	T	T	T	T	T	T	T	T	T	T	T	T	T	T	T	T
Met48		T(2)	T	T	T	T	T	T	T	T	T	T	T	T	T	T	T	C	T	T	T	T	T	T	T	T	T
Gly49		T(2)	C	T	T	C	C	C	C	T	C	C	C	C	C	T	C	C	C	C	C	T	C	C	C	C	T
Gly50		T(2)	C	T	T	C	C	C	C	T	C	C	C	C	C	T	C	C	C	C	C	C	C	C	C	C	C
Arg51	Arg51	T(2)	T	T	T	C	C	C	C	T	C	C	C	C	C	T	C	C	C	C	C	C	T	C	C	C	C
Pro52		T(2)	T	T	T	C	C	C	C	T	C	C	C	C	C	T	C	C	C	C	C	C	T	C	C	C	C
Arg53		B(4)	B	B	B	B	C	B	C	B	B	B	B	B	B	B	C	C	C	B	B	C	B	B	B	B	B
Glu54		B(4)	B	B	B	B	B	B	C	B	B	B	B	B	B	B	C	C	B	B	B	B	B	B	B	B	B
Asp55		B(4)	B	B	B	B	B	B	B	B	B	B	B	B	B	B	B	Bb	B	B	B	B	B	B	B	B	B
Arg56	Arg56	B(4)	B	B	B	B	B	B	B	B	B	B	B	B	B	B	B	C	B	B	B	B	B	B	B	B	B
Val57		B(4)	B	B	B	B	B	B	B	B	B	B	B	B	B	B	B	C	B	B	B	B	B	B	B	B	B
Pro58		T(3)	T	T	T	T	T	T	T	T	T	T	T	T	T	T	T	C	T	T	T	C	C	C	C	C	C
Pro59		T(3)	T	T	T	T	T	T	T	T	T	T	T	T	T	T	T	C	T	T	T	T	C	T	T	T	T
Ser60		T(3)	T	T	T	T	T	T	T	T	T	T	T	T	T	T	T	C	T	T	T	T	C	T	T	T	T
Arg61		T(3)	T	T	T	T	T	T	T	T	T	T	T	T	T	T	T	C	T	T	T	T	C	T	T	T	T
Asn62		C(4)	T	C	C	C	C	T	T	T	C	T	T	T	C	C	C	C	C	T	T	T	C	T	T	T	T
Ser63		B(5)	B	B	B	C	C	B	B	T	C	T	T	T	B	C	C	B	B	T	B	B	B	B	B	B	B

Ile64	B(5)	B	B	B	C	B	B	B	B	B	T	T	B	B	B	C	B	B	T	B	B	B	B	B	B	B
Thr65	B(5)	B	B	B	C	B	B	B	B	B	B	Bb	B	B	B	Bb	B	B	Bb	B	B	B	B	B	B	B
Leu66	B(5)	C	B	B	C	B	B	B	T	C	B	C	T	T	T	C	T	C	C	C	B	C	C	C	B	C
Thr67	C(5)	C	C	C	C	B	C	C	T	T	C	C	T	T	T	C	T	C	C	C	C	C	C	C	C	C
Asn68	C(5)	C	C	C	C	C	C	C	T	T	C	C	T	T	T	T	T	C	C	C	C	C	C	C	C	C
Leu69	C(5)	C	C	C	C	C	C	C	T	T	C	C	T	T	T	T	T	C	C	C	C	C	C	C	C	C
Asn70	T(4)	T	T	T	T	T	T	T	C	C	C	C	C	T	T	T	T	T	T	C	T	T	T	T	T	T
Pro71	T(4)	T	T	T	T	T	T	T	C	C	C	C	C	T	T	T	T	T	T	C	T	T	T	T	T	T
Gly72 Gly72	T(4)	T	T	T	T	T	T	T	C	C	C	C	C	T	T	C	T	T	T	C	T	T	T	T	T	T
Thr73	T(4)	T	T	T	B	B	T	T	C	C	C	C	C	T	T	B	T	B	T	C	B	B	T	T	B	B
Glu74	B(6)	C	B	B	B	B	B	B	B	B	B	C	B	B	B	B	B	B	B	B	B	B	C	B	B	B
Tyr75	B(6)	B	B	B	B	B	B	B	B	B	B	B	B	B	B	B	B	B	B	B	B	B	B	B	B	B
Val76	B(6)	B	B	B	B	B	B	B	B	B	B	B	B	B	B	B	B	B	B	B	B	B	B	B	B	B
Val77	B(6)	B	B	B	B	B	B	B	B	B	B	B	B	B	B	B	B	B	B	B	B	B	B	B	B	B
Ser78	B(6)	B	B	B	B	B	B	B	B	B	B	B	B	B	B	B	B	B	B	B	B	B	B	B	B	B
Ile79	B(6)	B	B	B	B	B	B	B	B	B	B	B	B	B	B	B	B	B	B	B	B	B	B	B	B	B
Val80	B(6)	B	B	B	B	B	B	B	B	B	B	B	B	B	B	B	B	B	B	B	B	B	B	B	B	B
Ala81	B(6)	B	B	B	B	B	B	B	B	B	B	B	B	B	B	B	B	B	B	B	B	B	B	B	B	B
Leu82	B(6)	B	B	B	B	B	B	B	B	B	B	B	B	B	B	B	B	B	B	B	B	B	B	B	B	B
Asn83	B(6)	T	B	B	C	B	B	B	T	T	B	T	B	C	T	T	T	T	T	B	T	T	T	B	T	T
Ser84	T(5)	T	T	T	C	T	T	T	T	T	T	T	T	C	T	T	T	T	T	T	T	T	T	T	T	T
Lys85 Lys85	T(5)	T	T	T	C	T	T	T	T	T	T	T	T	C	T	T	T	T	T	T	T	T	T	T	T	T
Glu86	B(7)	T	B	B	C	B	B	B	T	T	B	T	B	C	T	T	T	T	T	B	T	T	T	B	T	T
Glu87	B(7)	Bb	B	B	T	B	B	B	B	B	B	B	B	C	Bb	Bb	B	Bb	Bb	B	B	Bb	Bb	B	Bb	Bb

Ser88		C(6)	C	C	C	T	B	C	B	B	B	B	B	C	C	C	C	B	C	C	C	B	C	C	C	C	C
Leu89		C(6)	C	C	C	T	B	C	B	B	B	B	B	C	C	C	C	B	C	C	C	B	C	C	C	C	C
Pro90		C(6)	C	C	C	T	B	C	B	B	B	B	B	C	C	C	C	B	C	C	C	B	C	C	C	C	C
Leu91		B(8)	B	B	B	B	B	B	B	B	B	B	B	B	B	B	B	B	B	B	B	B	B	B	B	B	B
Val92		B(8)	B	B	B	B	B	B	B	B	B	B	B	B	B	B	B	B	B	B	B	B	B	B	B	B	B
Gly93		B(8)	B	B	B	B	B	B	B	B	B	B	B	B	B	B	B	B	B	B	B	B	B	B	B	B	B
Gln94		B(8)	B	B	B	B	B	B	B	B	B	B	B	B	B	B	B	B	B	B	B	B	B	B	B	B	B
Gln95		B(8)	B	B	B	B	B	B	B	B	B	B	B	B	B	B	B	B	B	B	B	B	B	B	B	B	B
Ser96		B(8)	C	B	B	B	B	B	B	B	B	B	C	B	B	B	B	B	B	B	B	B	B	C	B	B	B
Thr97		C(7)	C	C	C	B	B	C	C	C	C	C	C	C	C	C	B	C	B	C	C	B	B	C	C	B	B
Val98		C(7)	C	C	C	C	C	C	C	C	C	C	C	C	C	C	C	C	C	C	C	C	C	C	C	C	C
Ser99	Ser99	C(7)	C	C	C	C	C	C	C	C	C	C	C	C	C	C	C	C	C	C	C	C	C	C	C	C	C

7. Accessibility to the Solvent

Recently, Eisenberg *et al*.,[3] based on experimental data, discussed how minute changes in the amino acid composition of a protein may affect the surface binding mode and differentiate the fate of cell cultures grown on media covered by FN. Antibodies, key players in popular immunochemical methods of detecting FN, seek also appropriate accessible epitopes on the exposed regions for selective binding to FN. To facilitate further analysis of possible molecular recognition processes,[4] we have listed residues exposed to the solvent after $FN^{III}9$ adsorption on each model surface (Tab. S4). In summary, the FN protein regions easily accessible upon adsorption are the following:

(i) on mica, the N- and C-ter, and entire B1 & B7 sheets. The exposed region is acidic and neutral in terms of hydrophobicity;

(ii) on our model positive ionic surface (SiO_2), the N-ter and entire B4 and B5 β-strands and parts of B3 and B6 β-strands. The region accessible from water solvent is basic and hydrophilic;

(iii) on Au{111}, a common trend is not detected because adsorption on gold is not as specific as on the other surfaces. The regions exposed are hydrophilic, and a large part of the protein is exposed to other proteins.

Thus the series of simulations presented here indicate that the nature of the surface to which $FN^{III}9$ adsorbs affects the regions exposed for possible interactions with integrins, antibodies and/or other FN ligands. These results should guide further work on the functionalization of surfaces for biomedical applications.

Table S4. Residues exposed to the solvent after 100ns adsorption trajectories of $FN^{III}9$ on mica (trajectories FNm, V1, …, V6), SiO_2 (trajectories $FNSiO_2$, V1, …, V6 and $FnpSiO_2$, V1, … , V6), and Au {111} (trajectories FNAu V1, … , V6) surface models. Residues exposed to the solvent are indicated by +, the secondary structure of the final protein conformation on the surface is colour-coded; grey, blue, yellow and red indicate a coil, turn, β-strand and β-bridge, respectively. In the second column the secondary structure of the $FN^{III}9$ initial structure is given, while numbering is provided in brackets.

Residue	Structure	Trajectory																							
		FNm						$FNSiO_2$						$FNpSiO_2$						FNAu					
		V1	V2	V3	V4	V5	V6	V1	V2	V3	V4	V5	V6	V1	V2	V3	V4	V5	V6	V1	V2	V3	V4	V5	V6
Ala8	C(1)						+	+	+	+	+	+	+	+	+	+	+	+	+	+	+		+	+	
Leu9	C(1)						+	+	+		+		+	+	+	+	+		+	+			+	+	
Asp10	C(1)	+					+							+	+	+	+		+	+	+		+	+	
Ser11	C(1)	+					+														+		+		
Pro12	C(1)						+																		
Thr13	B(1)	+			+		+														+			+	+
Gly14	B(1)	+			+		+																	+	+
Ile15	B(1)	+	+		+		+																		
Asp16	B(1)	+	+		+	+	+																	+	+
Phe17	B(1)		+	+	+	+	+																	+	+
Ser18	B(1)	+	+	+	+	+	+																	+	+
Asp19	C(2)	+	+	+	+	+	+															+		+	+
Ile20	C(2)	+	+	+	+	+	+															+		+	+
Thr21	T(1)	+	+		+	+	+																	+	+

Ala22	T(1)					+																+			+
Asn23	T(1)					+																+			+
Ser24	T(1)																							+	+
Phe25	B(2)																								
Thr26	B(2)																							+	+
Val27	B(2)																								
His28	B(2)																							+	+
Trp29	B(2)																							+	+
Ile30	B(2)	+			+		+													+	+			+	+
Ala31	C(3)																			+				+	+
Pro32	C(3)																			+				+	+
Arg33	C(3)	+					+			+	+	+	+	+	+	+		+	+	+		+	+	+	+
Ala34	C(3)								+	+	+	+	+	+	+	+		+	+	+		+	+		
Thr35	C(3)							+	+	+	+	+	+	+	+	+	+	+	+	+		+	+	+	+
Ile36	C(3)							+	+		+	+	+	+	+	+	+	+	+				+	+	+
Thr37	C(3)							+	+	+	+	+	+	+	+	+	+	+	+			+	+		
Gly38	B(3)							+	+	+					+				+						
Tyr39	B(3)																							+	
Arg40	B(3)							+	+	+	+	+	+	+	+	+	+	+	+		+		+		
Ile41	B(3)																								
Arg42	B(3)										+										+		+		
His43	B(3)																								
His44	B(3)																				+		+		
Pro45	B(3)																				+		+		

Glu46	T(2)	+	+	+		+	+													+		+			
Asn47	T(2)	+	+	+		+	+													+	+	+			
Met48	T(2)	+		+		+															+	+			
Gly49	T(2)																				+				
Gly50	T(2)										+											+			
Arg51	T(2)							+	+	+	+	+	+	+	+	+	+	+	+	+		+			
Pro52	T(2)								+	+	+		+	+		+	+		+	+		+			
Arg53	B(4)							+	+	+	+	+	+	+	+	+	+	+	+						
Glu54	B(4)							+	+	+	+	+	+	+	+	+	+	+	+	+		+			
Asp55	B(4)							+	+	+	+	+	+	+	+		+	+	+						
Arg56	B(4)								+	+	+	+	+	+	+	+	+	+	+	+					
Val57	B(4)							+		+		+	+	+		+	+		+						
Pro58	T(3)							+	+	+	+	+	+	+	+	+	+	+	+	+					
Pro59	T(3)							+	+	+	+	+	+	+	+	+	+	+	+	+					
Ser60	T(3)							+	+	+	+	+	+	+	+	+	+	+	+	+					
Arg61	T(3)							+	+	+	+	+	+	+	+	+	+	+	+	+					
Asn62	C(4)											+			+					+					
Ser63	B(5)											+	+	+	+		+								
Ile64	B(5)							+		+	+	+	+	+	+	+	+	+	+						
Thr65	B(5)							+		+	+	+	+	+	+	+	+	+	+						
Leu66	B(5)									+				+					+						
Thr67	C(5)							+			+	+	+	+	+	+	+	+	+						
Asn68	C(5)							+				+	+	+	+	+	+	+				+			
Leu69	C(5)																					+			

Asn70	T(4)			+		+																+			
Pro71	T(4)			+		+																+			
Gly72	T(4)	+	+	+	+	+																+			
Thr73	T(4)		+			+																+			
Glu74	B(6)	+	+	+	+	+																	+		
Tyr75	B(6)																								
Val76	B(6)																				+		+		
Val77	B(6)																								
Ser78	B(6)																				+		+		
Ile79	B(6)																								
Val80	B(6)																						+		
Ala81	B(6)																								
Leu82	B(6)							+	+	+	+	+	+	+	+	+		+	+	+	+		+		
Asn83	B(6)							+	+	+	+	+	+	+	+	+	+	+	+	+		+	+		
Ser84	T(5)							+	+	+	+	+	+	+	+	+	+	+	+	+		+	+		
Lys85	T(5)							+	+	+	+	+	+	+	+	+	+	+	+	+		+	+		
Glu86	T(5)							+		+	+	+	+	+	+	+	+	+	+	+		+	+		
Glu87	T(5)											+		+	+	+	+		+	+	+		+		
Ser88	C(6)																			+		+			
Leu89	C(6)	+					+													+		+			
Pro90	C(6)	+					+													+		+			
Leu91	B(7)	+			+		+													+					
Val92	B(7)	+			+		+													+		+			
Gly93	B(7)				+		+																		

Gln94	B(7)	+	+	+	+	+	+													+		+			
Gln95	B(7)	+	+	+	+	+	+																		+
Ser96	B(7)	+	+	+	+	+	+														+				+
Thr97	C(7)	+	+	+	+	+	+														+				+
Val98	C(7)	+	+	+	+	+	+														+				+
Ser99	C(7)	+	+	+	+	+	+														+				+

8. Structural Changes Upon Adsorption

$FN^{III}9$ is a mostly β structure protein[7] which contains 8 extended β structures (7 β-sheets and one short β structure, Tab. S3) connected by coils and turns which are responsible for the relatively significant intrinsic flexibility. As the RMSD plot shown in Fig. S5 indicates, even in water only the protein is relatively flexible and the RMSD reaches the value of about 2.6 Å, which is quite significant for a 92 residue-long protein. This observation agrees well with the $FN^{III}9$ softness.[3] The RSMD calculated for $FN^{III}9$ adsorbed at the mica and SiO_2 model surfaces appear to be slightly higher than in water only, but at the end of the trajectory it reaches a comparable level (Fig. S5 a). Most likely this is a reflection of local structural adjustments of the adsorbed protein. Surprisingly, in the case of adsorption at the Au{111} surface the RMSD is lower, fluctuating around 1.6 Å and 2 Å, depending on trajectory.

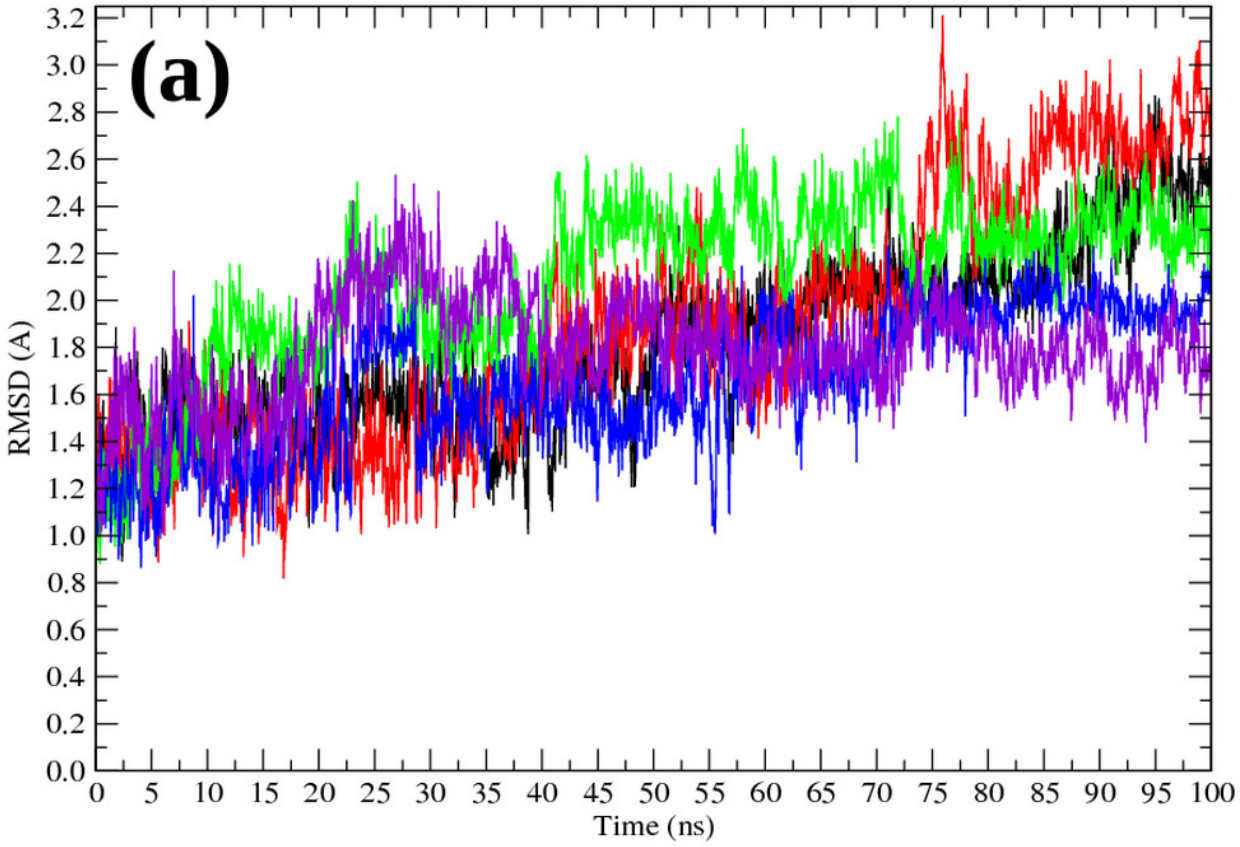

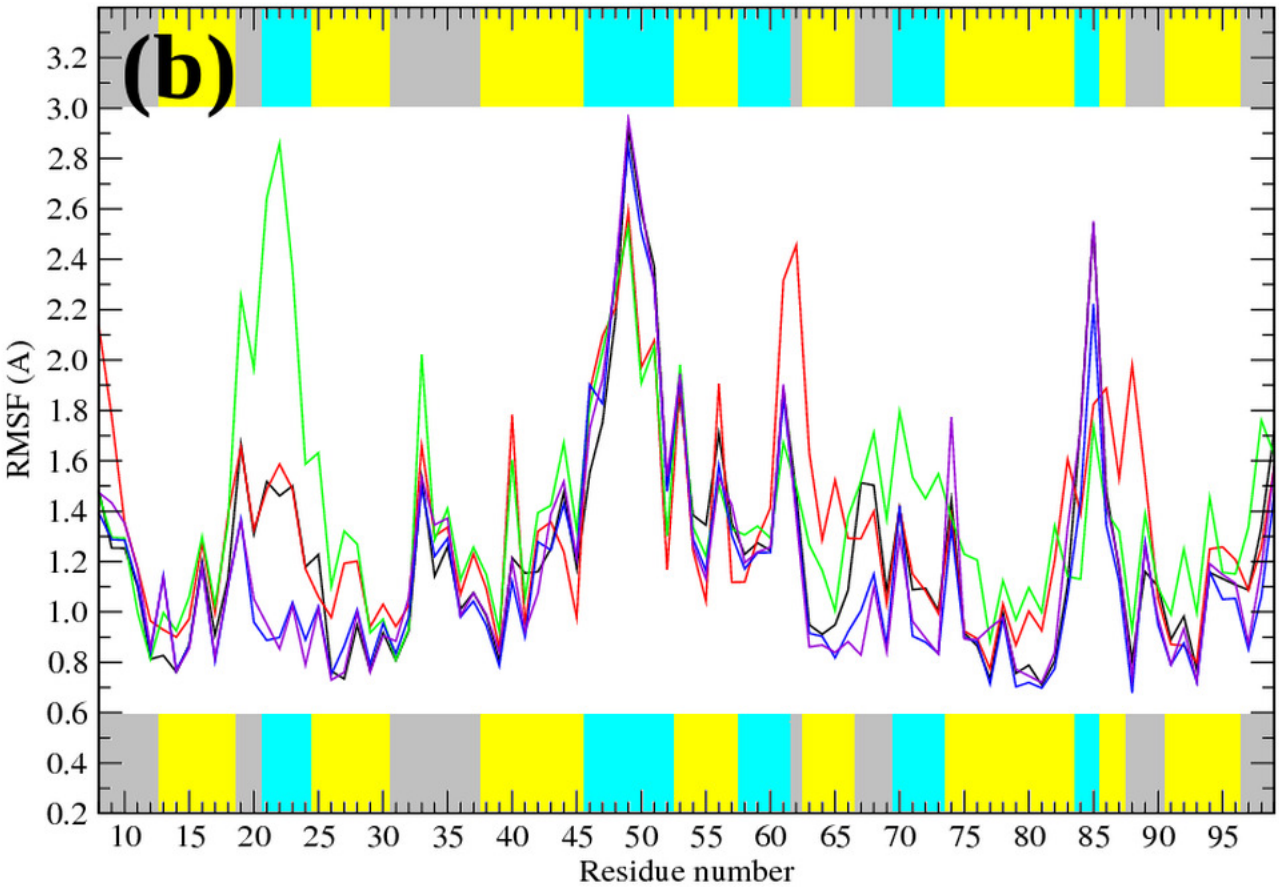

Figure S5. RMSD (a) and RMSF (b) plots during: 100 ns production trajectory in water (black), mica surface adsorption trajectory FNmV3 (red), SiO_2 surface adsorption trajectory FNSiO_2V5 (green), Au{111} surface adsorption trajectory FNAuV1 (blue) and FNAuV5 (purple). The color ribbon at the RMSF indicates secondary structure of initial FNIII9: coils are shown in gray, turns in cyan and extended β structures by yellow. In both cases the preparation period (minimization, heating and equilibration) is omitted. The RMSD and RMSF were calculated with respect to the initial $FN^{III}9$ structure.

As briefly mentioned in the above sections describing the adsorption mechanisms, the $FN^{III}9$ does not tend to unfold, and this observation is further confirmed by the analysis of residues' fluctuations around their average position in the trajectory (see the RMSF plot, Fig. S5 b). With only a few exceptions, the highest fluctuations appear at turn and coil regions, and the β structures are mostly intact. More details on the final secondary structure of $FN^{III}9$ after 100 ns trajectories can be found

in Tab. S3.

To gain a better insight into the range of structural changes caused by the adsorption we have prepared overlaps of initial and final (adsorbed) protein structures. Figure S6 shows structure overlaps for the representative trajectories in each category. As one can see, the biggest changes appear at turns and coils regions while the β structures overlaps very well.

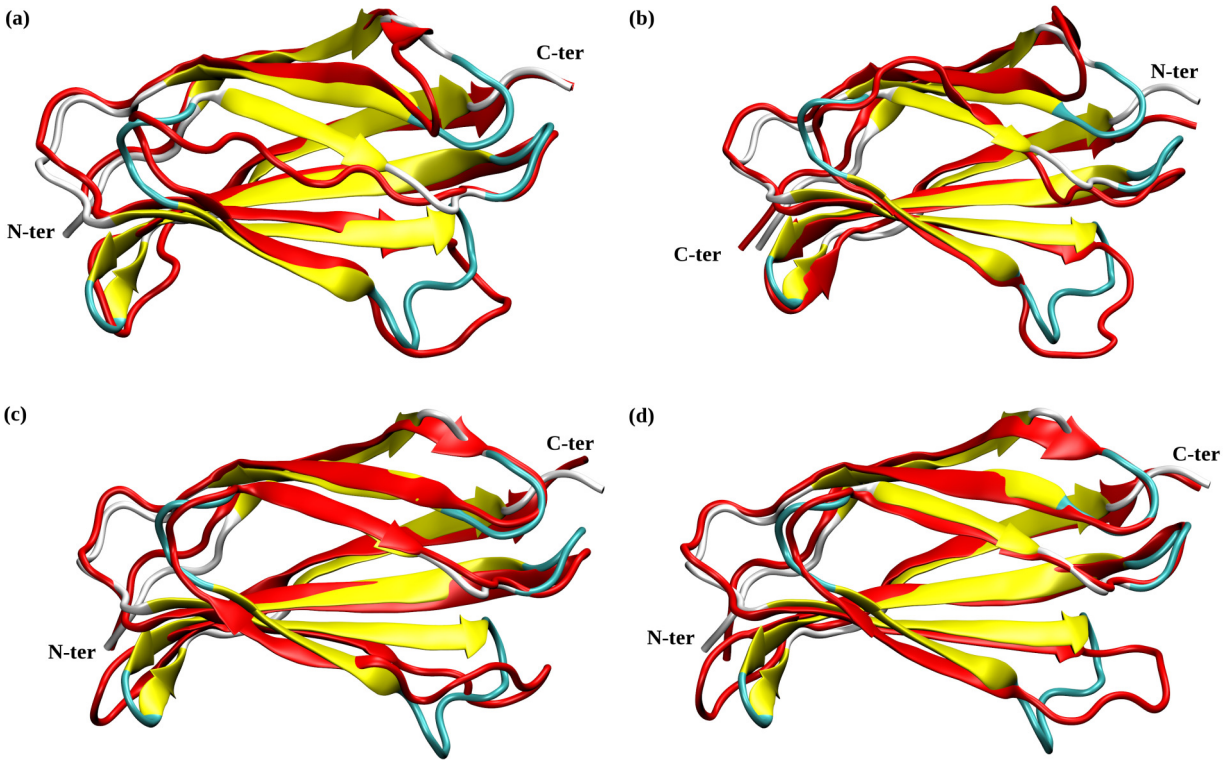

Figure S6. Overlap of the initial and final structure of FNIII9 obtained for representative trajectories. (a) FNmV3, (b) FNSiO2V5, (c) FNAuV1, (d) FNAuV5. Protein secondary structure is shown as a cartoon colored by structure type (initial structure) and in red (100 ns structure). Protein ends are annotated.

9. References

1. Patwardhan, S. V.; Emami, F. S.; Berry, R. J.; Jones, S. E.; Naik, R. R.; Deschaume, O.; Heinz, H.; Perry, C. C. Chemistry of Aqueous Silica Nanopatricle Surfaces and the Mechanism of Selective Peptide Adsorption. *J. Am. Chem. Soc.* **2012**, 134, 6244-6256.

2. Feng, J.; Pandey, R. B.; Berry, R. J.; Farmer, B. L.; Naik, R. R.; Heinz, H. Adsorption Mechanism of Single Amino Acid and Surfactant Molecules to Au {111} surfaces in Aquaeous Solution: Design Rules for Metal-Binding Molecules. *Soft Matter*, **2011**, 7, 2113-2120.

3. Eisenberg, J. L.;, Piper J. L.; Mrksich M. Using Self-Assembled Monolayers to Model Cell Adhesion 10th Type III Domains of Fibronectin, *Langmuir*, **2009**, 25, 13942–13951.

4. Lekka M., Kulik A.J., Lee K., Pyka-Fościak G., Nowak W. Probing fibronectin-Antibody Interaction Using AFM Force Spectroscopy and Lateral Force Microscopy. *J. Chem. Phys*, **2013,** Submitted.

5. Schiefner, A.; Gebauer, M.; Skerra, A. Extra-domain B in Oncofetal Fibronectin Structurally Promotes Fibrillar Head-to-tail Dimerization of Extracellular Martix Protein. J. *Biol. Chem.* **2012**, 287, 17578-17588.6. Henderson, B.; Nair, S.; Pallas, J.; Williams, M. A. Fibronectin: a Multidomain Host Adhesin Targeted by Bacterial Fibronectin-Binding Proteins. F*EMS Microbiol. Rev.* **2011**, 35, 147-200.